Article

Current Biology

Acclimation of Oxygenic Photosynthesis to Iron Starvation Is Controlled by the sRNA IsaR1

Graphical Abstract

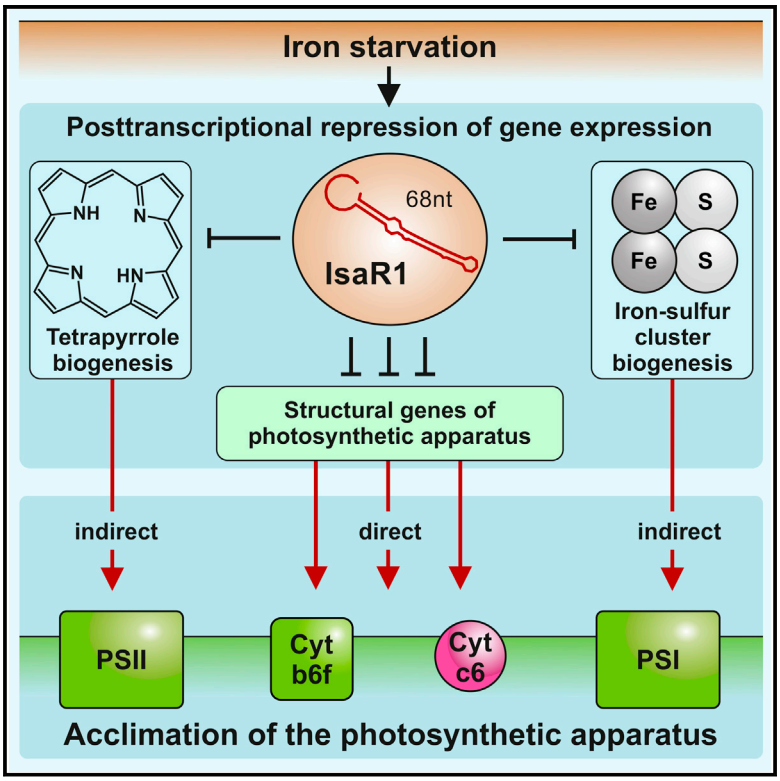

Highlights

- IsaR1 controls the synthesis of photosynthetic electron transport components
- IsaR1 maintains the regulation of Fe/S cluster biogenesis when iron is limiting
- Synthesis of chlorophylls, heme, and phycocyanin is controlled at an early step
- IsaR1 plays a major role in the response to iron starvation

Authors

Jens Georg, Gergana Kostova, Linda Vuorijoki, ..., Matthias E. Futschik, Eva-Mari Aro, Wolfgang R. Hess

Correspondence

wolfgang.hess@biologie.uni-freiburg.de

In Brief

Oxygenic photosynthesis requires iron cofactors, making photosynthetic cells one of the most iron-rich cellular systems. Georg et al. show that the cyanobacterial sRNA IsaR1 is induced under iron starvation and then acts on the photosynthetic apparatus in three specific ways. IsaR1 controls a complex network relevant for acclimation to low iron.

Georg et al., 2017, Current Biology 27, 1425–1436
May 22, 2017
http://dx.doi.org/10.1016/j.cub.2017.04.010

CellPress

Current Biology
Article

Acclimation of Oxygenic Photosynthesis to Iron Starvation Is Controlled by the sRNA IsaR1

Jens Georg,[1] Gergana Kostova,[1,6] Linda Vuorijoki,[2] Verena Schön,[1,7] Taro Kadowaki,[3] Tuomas Huokko,[2] Desirée Baumgartner,[1] Maximilian Müller,[1,8] Stephan Klähn,[1] Yagut Allahverdiyeva,[2] Yukako Hihara,[3] Matthias E. Futschik,[4,5] Eva-Mari Aro,[2] and Wolfgang R. Hess[1,9,*]

[1]Genetics & Experimental Bioinformatics, Institute of Biology III, Faculty of Biology, University of Freiburg, Schänzlestrasse 1, 79104 Freiburg, Germany
[2]Molecular Plant Biology, Department of Biochemistry, University of Turku, 20014 Turku, Finland
[3]Graduate School of Science and Engineering, Saitama University, Saitama 338-8570, Japan
[4]CCMAR - Center of Marine Sciences, University of Algarve, Campus de Gambelas, 8005-139 Faro, Portugal
[5]School of Biomedical and Healthcare Sciences, Plymouth University, Plymouth, Devon PL4 8AA, UK
[6]Present address: CNRS UMR8261, Institut de Biologie Physico-Chimique, 13 rue Pierre et Marie Curie, 75005 Paris, France
[7]Present address: Department of Ecogenomics and Systems Biology, University of Vienna, Althanstrasse 14, 1090 Vienna, Austria
[8]Present address: Institute for Cell and Gene Therapy, University of Freiburg, Breisacher Strasse 115, 79106 Freiburg, Germany
[9]Lead Contact
*Correspondence: wolfgang.hess@biologie.uni-freiburg.de
http://dx.doi.org/10.1016/j.cub.2017.04.010

SUMMARY

Oxygenic photosynthesis crucially depends on proteins that possess Fe^{2+} or Fe/S complexes as co-factors or prosthetic groups. Here, we show that the small regulatory RNA (sRNA) IsaR1 (Iron-Stress-Activated RNA 1) plays a pivotal role in acclimation to low-iron conditions. The IsaR1 regulon consists of more than 15 direct targets, including Fe^{2+}-containing proteins involved in photosynthetic electron transfer, detoxification of anion radicals, citrate cycle, and tetrapyrrole biogenesis. IsaR1 is essential for maintaining physiological levels of Fe/S cluster biogenesis proteins during iron deprivation. Consequently, IsaR1 affects the acclimation of the photosynthetic apparatus to iron starvation at three levels: (1) directly, via posttranscriptional repression of gene expression; (2) indirectly, via suppression of pigment; and (3) Fe/S cluster biosynthesis. Homologs of IsaR1 are widely conserved throughout the cyanobacterial phylum. We conclude that IsaR1 is a critically important riboregulator. These findings provide a new perspective for understanding the regulation of iron homeostasis in photosynthetic organisms.

INTRODUCTION

Oxygenic photosynthesis requires iron cofactors, e.g., in its electron transfer systems, within the numerous Fe/S cluster-containing proteins and particularly in photosystem I (PSI). Thus, the photosynthetic apparatus is one of the most iron-rich cellular systems. The PSI complexes of the model cyanobacterium *Synechocystis* sp. PCC 6803 (hereinafter *Synechocystis* 6803) were estimated to contain 1.2×10^6 iron atoms per cell, about one order of magnitude more iron than an average *E. coli* cell [1, 2]. Consequently, photosynthesis is fundamentally vulnerable to iron starvation, a situation that occurs frequently in nature [3]. However, the control of iron starvation responses is only partially understood in plants and phototrophic microorganisms.

Physiologically, the photosynthetic apparatus becomes strongly remodeled upon iron limitation [4–6]. The amounts of phycocyanin and chlorophyll become lowered [7, 8], and photosynthetic intersystem electron transport is restricted [5]. Iron-containing proteins are substituted or reduced, including cytochrome b-559 of photosystem II (PSII) (*psbEF* gene products), cytochromes b and f of the cytochrome b_6f complex, and all the Fe/S cluster proteins, especially those of PSI [8–10].

Upon iron starvation, cyanobacteria reduce the relative number of PSI complexes from a 4:1 PSI:PSII ratio to a 1:1 ratio (for an overview, see [6]) and induce the chlorophyll-binding iron-stress-induced protein A [11, 12]. Iron depletion triggers the expression of proteins involved in iron transport and mobilization, such as FutABC, FeoB, and ferritin [13] and of alternative redox carriers, including copper-dependent plastocyanin (*petE* gene) and flavodoxin (*isiB* gene product), which replace their iron-dependent counterparts cytochrome *c*553 or *c*6 (*petJ* gene) and ferredoxin 1 (Fed1) [9, 14].

Studies of iron homeostasis in non-photosynthetic bacteria revealed two key players involved in its regulation: the ferric uptake regulator (Fur), a transcription factor commonly considered a transcriptional repressor when bound to Fe^{2+}, and a small regulatory RNA (sRNA), in enterobacteria called RyhB, which is controlled by Fur [15]. At higher iron concentrations, Fur binds Fe^{2+} to its regulatory site, leading to its dimerization, activation, and DNA binding at specific DNA sequences, the Fur boxes in the promoter regions of relevant genes [16]. At lower iron concentrations, Fur loses the bound Fe^{2+}; becomes inactive; detaches from the DNA; and in *Synechocystis* 6803, it is eventually degraded by FtsH3 protease [17], and transcription of its target genes is derepressed. However, in cyanobacteria, there is no evidence that any of the characterized transcription factors, including FurA [18], would directly impact

the expression of genes in the photosynthetic electron transport chain.

Therefore, we focused on sRNAs that would become specifically induced in this condition as potential functional analogs of RyhB. In *Synechocystis* 6803, an sRNA initially called NC-181 or Ncl1600 becomes highly induced upon iron deficiency [19, 20]. We renamed this 68-nt sRNA as Iron-Stress-Activated RNA1 (IsaR1). Here, we comprehensively characterize the function of IsaR1 and demonstrate that IsaR1 has an essential regulatory role in the acclimation of the photosynthetic apparatus to iron starvation.

RESULTS

The sRNA IsaR1 Is Widely Distributed in the Cyanobacterial Phylum

The sRNA IsaR1 in *Synechocystis* 6803 originates from the intergenic spacer between the *sll0033* gene encoding carotene isomerase CrtH and *sll0031* encoding the circadian-clock-related light-dependent period modulator protein A (LdpA).

IsaR1 is widely conserved among N_2 fixing, unicellular and filamentous, freshwater, marine, symbiotic, mesophilic, and thermophilic cyanobacteria (Figure S1). In most genomes, *isaR1* is associated with the genes encoding uracil phosphoribosyltransferase (*upp*), carotene isomerase (*crtH*), or both (Figure S1A). IsaR1 sequences are characterized by a highly conserved region within the 5′ segment and a sequence resembling a Rho-independent terminator of transcription (Figure S1B). This wide conservation of sequence, structure, and synteny suggests a conserved function for IsaR1 in cyanobacteria.

Expression of IsaR1 Is Specifically Enhanced by Iron Starvation and Is under the Transcriptional Control of Fur

Northern blot experiments verified the strong expression of IsaR1 during iron starvation but weak or negligible expression under the other conditions tested (Figure S1C). Promoter fusion experiments revealed that IsaR1 expression is induced by iron starvation and that the dynamics resembled the activation of the *isiA* promoter (Figure S2A). Indeed, the alignment of the *isaR1* upstream sequences from 31 cyanobacteria (Figure S2B) indicated the presence of a conserved sequence element resembling the Fur-binding site for *isiA* [21]. In addition, the demonstration of the specific binding of recombinant FurA to the IsaR1 promoter (P_{isaR1}) and its loss upon the replacement of likely critical residues in the conserved sequence supported the importance of this site for FurA-mediated regulation (Figure S2C).

Phenotypical Characterization of the IsaR1 Deletion and Complementation Mutants

A knockout mutant Δ*isaR1* in which *isaR1* was replaced by a kanamycin resistance gene and an inducible complementation strain, IsaR1comp, were subjected to iron starvation for 8 days by adding the iron chelator desferrioxamine B (DFB), while the P_{petE}-driven expression of IsaR1 in the complementation strain was induced by the addition of copper. Room temperature absorption spectra showed a stronger depigmentation in Δ*isaR1* than in the control (WT_pVZ) and the complemented strain IsaR1comp (Figures 1A–1C). The complemented strain was phenotypically more like wild-type (WT) than Δ*isaR1*; the slight spectral differences between WT and IsaR1comp likely resulted from using the weaker ectopic P_{petE} promoter.

To identify possible effects on the photosynthetic apparatus, the impact of ectopic IsaR1 expression under non-stress conditions was studied in a time course experiment. For this purpose, the vector with an extrachromosomal *isaR1* copy was introduced into *Synechocystis* 6803 WT, yielding the overexpressing strain IsaR1OE. Addition of Cu^{2+} induced the expression of IsaR1 from the copper-responsive P_{petE} promoter, while the iron concentration remained unchanged. Measuring the 77-K fluorescence emission spectra of IsaR1OE and the WT_pVZ control before and after 2, 4, 8, and 11 days of induction revealed an increase in the ratio between the 685-nm and 726-nm peaks (corresponding to the PSII/PSI ratio) over time in IsaR1OE (Figure 1D). This result resembles the characteristic increase in the PSII/PSI ratio under iron depletion due to the decline in the amount of PSI complexes [4, 22]. Only a slight decrease in the maximum quantum yield of PSII (defined as Fv/Fm) was observed in IsaR1OE (~25%), compared with WT_pVZ after 4 days of induction (Figure 1F). The Pm value, representing the maximum amount of photooxidizable P700, the primary donor of PSI, was less than half in IsaR1OE (Figure 1E). Moreover, the performance of PSI under actinic light, measured as the effective photochemical yield of PSI, was remarkably lower in IsaR1OE than in the control (Figure 1G). Importantly, the decrease in PSI yield was accompanied by a higher acceptor side limitation of PSI in IsaR1OE (Figure 1H).

Characterization of the Transcriptomic Response to Iron Depletion in the IsaR1 Deletion Mutant Reveals a Highly Altered Iron Stress Response

We compared Δ*isaR1* transcriptomes in a time course experiment after the induction of iron starvation to the published *Synechocystis* 6803 WT response [20] (Data S1 and S2). Despite its weak expression under iron-sufficient conditions (Figure S1C), the deletion of *isaR1* had a broad impact on the transcriptome (Figure 2A). The differentially abundant transcripts are presented in Table S1 according to operons and encoded functions and include transcripts related to the uptake of inorganic carbon (C_i), the C_i-limitation-responsive *flv4-flv2* (*sll0217-sll0219*) flavodiiron protein operon, the NADPH dehydrogenase complex, motility, and nitrogen assimilation and metabolism (Figure 2A). These results indicate a shift in the C-N metabolism in Δ*isaR1* and suggest a possible regulative role of IsaR1 under iron-replete conditions.

Whereas the levels of transcripts related to C_i, nitrogen assimilation, and NADPH dehydrogenase converged during prolonged iron starvation in both strains, notable differences in the transcriptional response to iron stress appeared, as illustrated by the 48-hr time point (Figure 2B). In agreement with the pronounced decreases in chlorophyll- and phycobilisome-dependent absorption in Δ*isaR1* at 48 hr of iron depletion (Figure 1), the transcript levels of photosynthesis-related genes encoding allophycocyanin, phycocyanin, and PSI and PSII components declined. In contrast, mRNAs for RNase E and RNase J, transposases, *psbZ*, *rpoE*, several iron-containing proteins (*sodB*, *acnB*, *ssl0020*/*petF*, and *sll1348*), and the Fe/S cluster biogenesis operon (*sufBCDS*) had stronger expression in the *isaR1* knockout strain. The genes with the strongest positive changes in Δ*isaR1* belonged to the

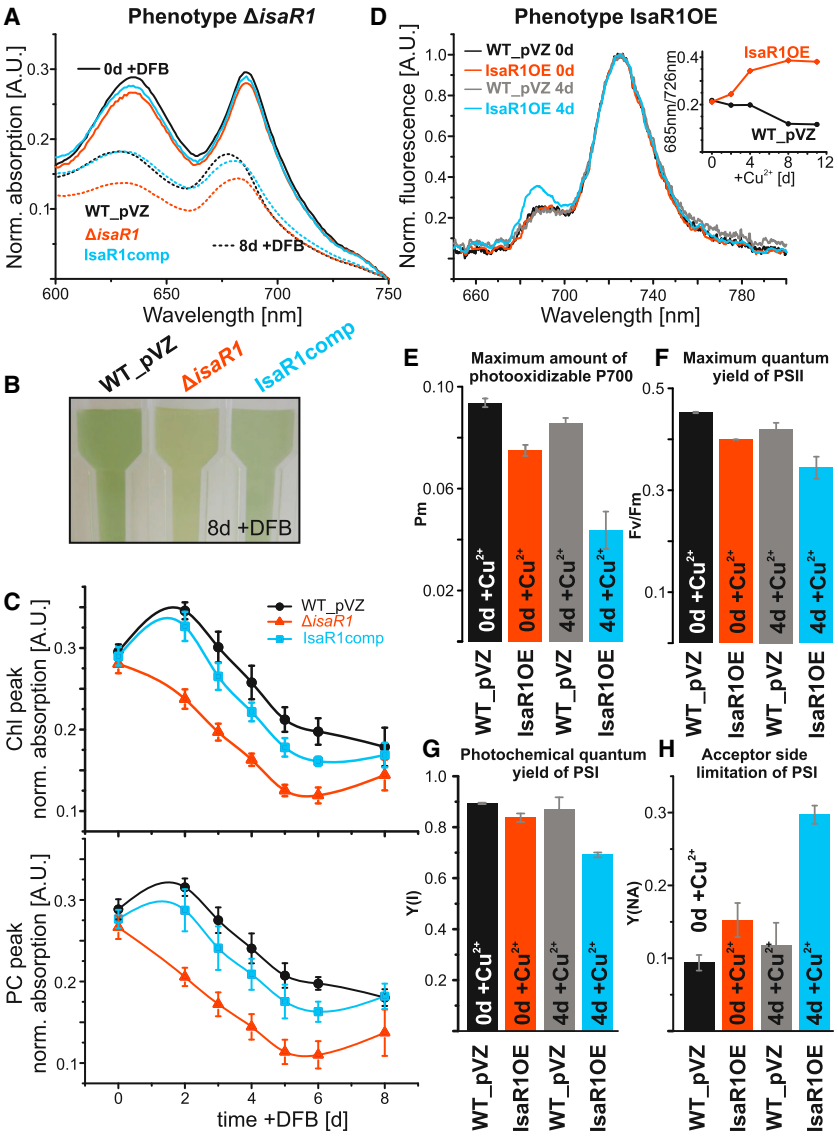

Figure 1. Phenotypes of Δ*isaR1* and IsaR1 Complementation and Overexpression Strains Compared with the Control Strain WT_pVZ, a WT Carrying the Empty Plasmid pVZ322::pPetE::oop

(A) Room temperature absorption spectra of WT, Δ*isaR1*, and IsaR1comp cell cultures before (0 days [d], continuous lines) and after (8 days, broken lines) the addition of 100 μM DFB (iron chelator) and 2 μM $CuSO_4$ (induction of the P_{petE} promoter for the complementation of IsaR1). The results from three independent biological replicates were averaged. The spectra were normalized (Norm.) to optical density 750 (OD_{750}) to help evaluate their structure.

(B) WT, Δ*isaR1*, and IsaR1comp cell cultures 8 days after the start of iron depletion.

(C) Decrease of chlorophyll (Chl) and phycocyanin (PC) absorptions in WT, Δ*isaR1*, and IsaR1comp cell cultures during iron limitation. Phycocyanin peak absorption was measured at 635 nm. Because of the blue shift of the chlorophyll peak during iron limitation, the chlorophyll absorption maximum wavelength changed from 686 nm to 678 nm. The error bars were calculated on the basis of three independent biological replicates.

(D) The 77-K fluorescence spectra of IsaR1OE and WT_pVZ before induction (0 days) and 4 days after induction with 2 μM $CuSO_4$. The fluorescence spectra were measured at 440 nm excitation. The chlorophyll content of the samples was adjusted to 7.5 μg Chl a/mL. The fluorescence spectra were normalized to 726 nm (PSI). Inset, top right: – 685-nm/726-nm peak ratio (indicating PSII:PSI ratio) in IsaR1OE and WT_pVZ control over the course of induction.

(E) Maximum amount of oxidizable P700 (Pm) before and after 4 days of IsaR1 induction (two biological replicates).

(F) The maximum quantum yield of PSII (Fv/Fm) in the presence of 20 μM DCMU (two biological replicates).

(G) Effective photochemical quantum yield of PSI, Y(I).

(H) Acceptor side limitation of PSI, Y(NA), in WT_pVZ and IsaR1OE before and after 96 hr of IsaR1 induction. Error bars indicate mean ± SD, two biological replicates.

ssr3570-3572kpsMT operon, which is possibly involved in extracellular lipopolysaccharide formation [23].

Computational Target Prediction and Analysis of Pulsed Overexpression Suggest Primary Targets of IsaR1

To elucidate the mode of action of IsaR1, we applied CopraRNA [24] using 20 IsaR1 homologs from various cyanobacteria to computationally predict IsaR1 targets. Functional enrichment analysis revealed a set of 38 candidate genes possibly controlled by IsaR1, belonging to the terms "iron ion containing," "electron transport," "metal ion binding, "photosynthesis," "iron-sulfur cluster binding," and proteins with GAF domains (Figure 3A). To enable the detection of *Synechocystis* 6803-specific targets that might have been missed by CopraRNA, we also compared the respective IntaRNA prediction [24] with the microarray results (Data S2).

We compared the transcriptome composition in IsaR1OE with an empty-vector control strain (WT_pVZ) at 6 hr after *isaR1* induction, when it was ~25-fold overexpressed (Figure S3). Potential targets are shown in Figure 4. The complete array results are summarized in Data S2 and visualized in Data S3.

Excluding IsaR1, 41 transcripts had lower and 19 had higher expression in IsaR1OE. The upregulation of several C_i-uptake-specific transcripts and of the mRNAs for glutamine-synthetase-inactivating factors *gifA* and *gifB* indicates a possible pleiotropic physiological response or shift in the C:N balance. Several mRNAs and 5′ UTRs among the 41 lower-expression target candidates were linked to photosynthesis and iron-containing proteins. In addition to the PSI-associated Fed1 (*petF*, *ssl0020*), mRNAs affected by IsaR1 overexpression included the cytochrome b_6f complex (*petD*, *petB*, and *petA*), the iron-containing superoxide dismutase (*sodB*), the enzyme that performs the first specific step of tetrapyrrole biosynthesis (*hemA*), cyanoglobin (*slr2097*), the SufC subunit of the Suf Fe/S-cluster biogenesis complex (*ycf16*), and some unknown or hypothetical proteins. The response regulators encoded by *sll1291* (TaxP2), *slr1594*

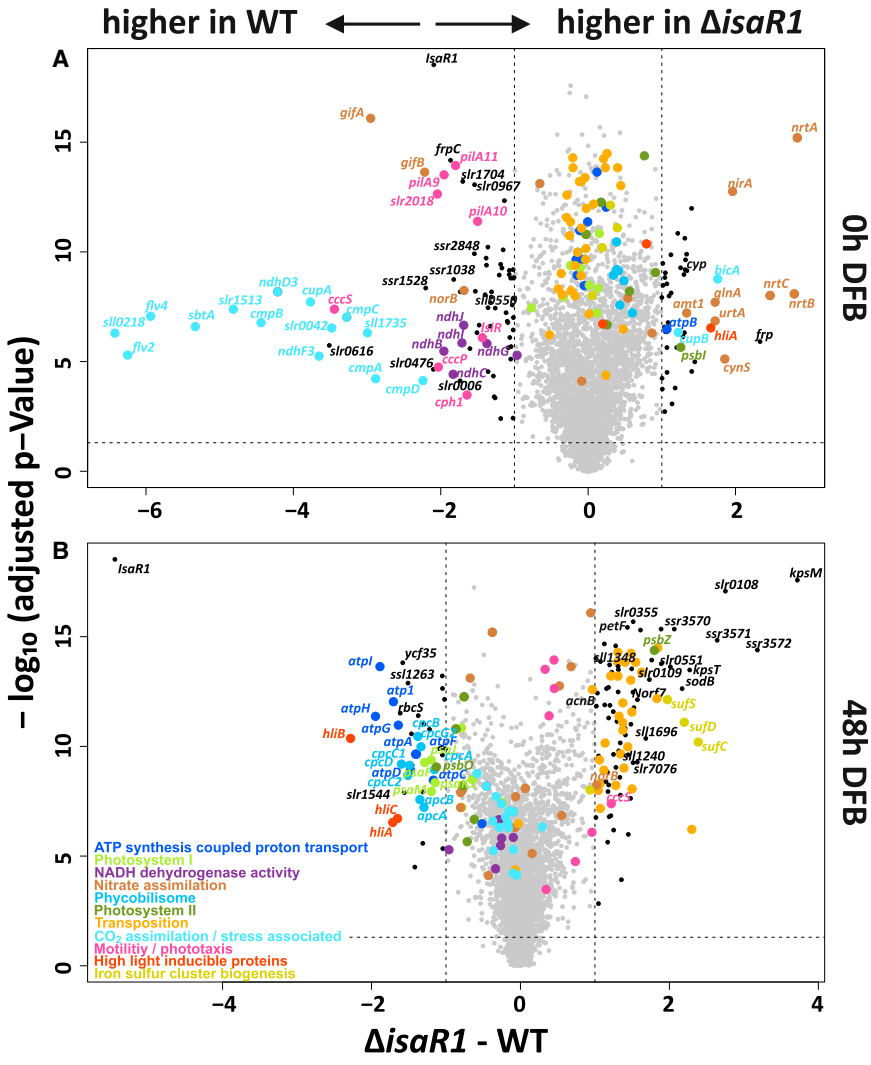

Figure 2. Transcriptome Differences between Δ*isaR1* and WT under Standard Conditions and after 48 Hr of Iron Depletion by DFB Addition

Transcriptome differences between Δ*isaR1* and WT under standard conditions (A) and after 48 hr of iron depletion by DFB addition (B). Volcano plots: log-transformed fold changes (FCs) between ΔisaR1 and WT (x axis, difference of $\log_2$ expression values) and $-\log_{10}$ (adjusted p value) (y axis). Broken lines indicate the adjusted p value threshold of 0.05 and FC thresholds of 1 and −1. Functional groups are color coded. Functional characterization was performed for all genes in the ΔisaR1-WT comparison with a significant FC at one or more of the time points after DFB addition (0 hr, 3 hr, 12 hr, 24 hr, 48 hr, or 72 hr). The differentially abundant transcripts were sorted according to operons and encoded functions in Table S1. Details are shown in the genome-wide expression plot (Data S1), and numeric values are presented in Data S2. See also Table S1 and Data S1 and S2.

and *slr1214* (LsiR), and the CU-pili-associated *slr1667* gene all were expressed at a lower level in IsaR1OE. An inverse relationship was identified between the higher accumulation of the 5′ UTR of *slr0074*-encoding SufB of the Fe/S cluster biosynthesis complex and the mRNA, which was slightly decreased (Figure 4).

After the integration of the previous data, we investigated the following groups in molecular detail: (1) the mobile electron carrier gene *petF1*; (2) the iron-sulfur cluster biogenesis genes, *sufBCDS*; (3) the genes of the four major subunits of the cytochrome b_6f complex, *petC1*, *petA*, *petB*, and *petD*; (4) genes involved in chlorophyll and tetrapyrrole biosynthesis, *hemA*, *chlH*, and *chlN*; and (5) genes for non-essential iron containing proteins such as *sodB*, *acnB*, and *ilvD*.

Selected Reaction Monitoring for Studying IsaR1 Target Proteins

Changes at the RNA level do not necessarily lead to changed protein abundances. To study the effects of IsaR1 deletion and overexpression on the protein profiles of the iron-depleted and iron-repleted cells, quantitative selected reaction monitoring (SRM)-based proteomics tailored to *Synechocystis* 6803 [10] was applied. SRM enables the precise quantification also of low-abundance proteins and of membrane proteins even from unfractionated samples. We quantified the four proteins encoded by the *suf*-operon (SufBCDS), their transcriptional regulator SufR [25], several other possible IsaR1 targets, and a set of control proteins. Altogether, the expression levels of 42 proteins in IsaR1OE and WT_pVZ, as well as in Δ*isaR1* (Tables S5 and S6) and the WT control, were investigated using SRM in two independent time course experiments (0, 24, and 96 hr after inducing IsaR1 overexpression and 0, 5, 24, 48, and 96 hr after the depletion of iron by DFB addition). To allow time for translation, an offset for the proteomics was chosen in comparison with the transcriptomic analysis. The respective $\log_2$-fold changes (FCs) of the detected protein levels in IsaR1OE compared with WT_pVZ are represented in Figure 3B and the specific results are described later, in context with the other data.

PSI-Associated Ferredoxin I Is a Major Target of IsaR1

The mRNA-encoding Fed1 (*petF*) was predicted as the highest-ranking IsaR1 target by CopraRNA (Figure 3A; Data S2). Consistent with this prediction, the typical strong downregulation of *petF* transcript accumulation under iron deprivation was missing in Δ*isaR1* (Figure 5A). Furthermore, the ectopic overexpression of IsaR1 under iron-replete conditions led to the rapid disappearance of *petF* mRNA (Figure 4) and a corresponding reduction of the Fed1 protein to less than 30% of the initial value at 96 hr after the induction of IsaR1, whereas the WT control did not show a reduction (Figure 5B).

The IntaRNA prediction suggested an extended interaction between IsaR1 and the *petF* 5′ UTR, including the

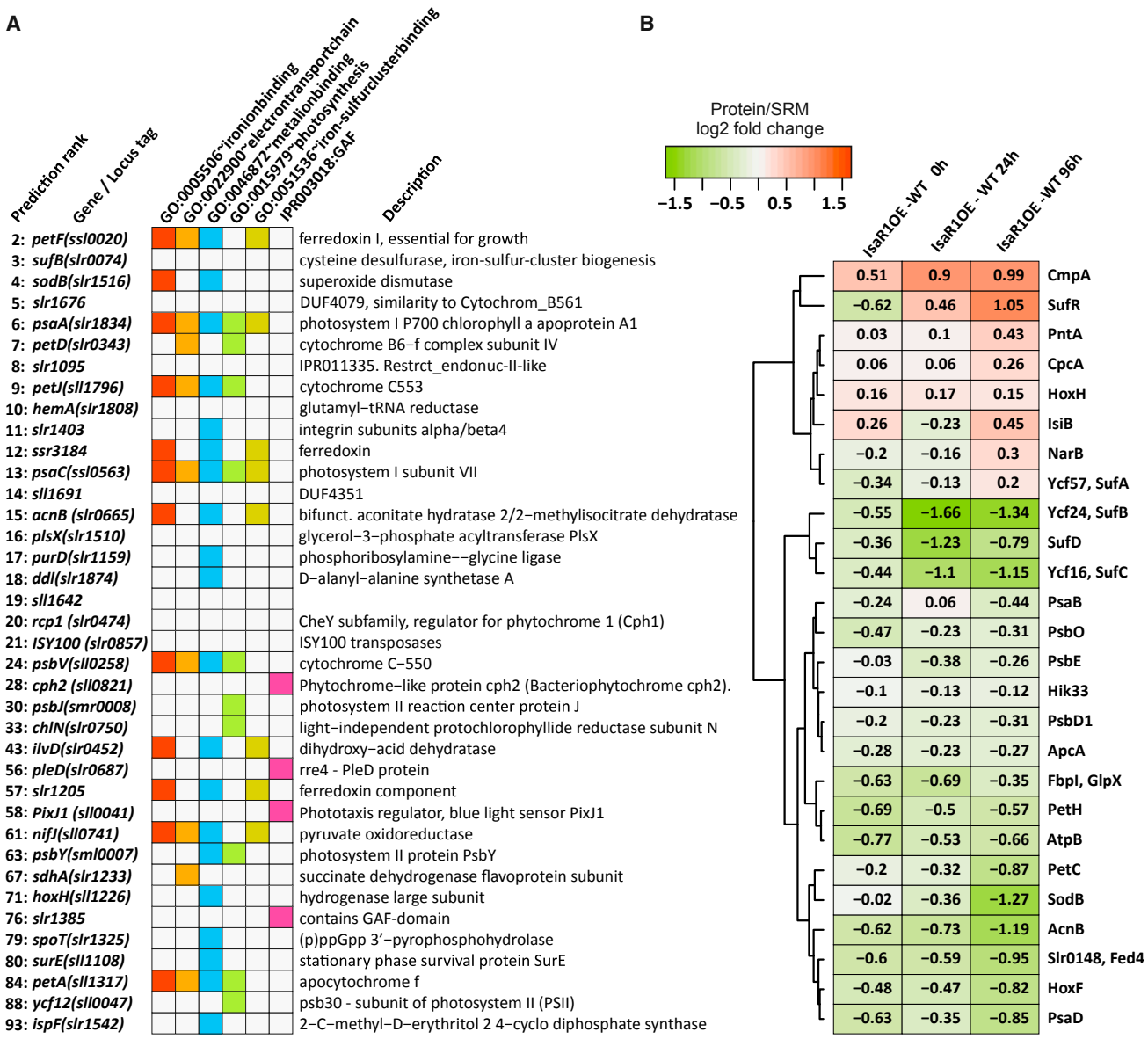

Figure 3. Prediction of IsaR1 Targets

(A) CopraRNA target prediction for IsaR1. The 38 most promising predicted targets are shown, including the top 20 predictions and those in the top-100 list that were enriched in one of the six displayed functional groups. The complete prediction is presented in Data S2. The top-ranking target, *upp*, was excluded because its 5′ UTR is located directly antisense to *isaR1* in many cyanobacteria, leading to an artificially good prediction p value. This is different in *Synechocystis* 6803; hence, we excluded *upp* from our analysis.

(B) Results of SRM proteomics of the IsaR1OE time course 0, 24, and 96 hr after induction. Only proteins with an adjusted p value ≤ 0.05 at time point 96 hr and absolute $\log_2$FC< 0.8 at time point 0 hr are displayed. The differentially abundant proteins are given in Table S2 according to operons and encoded functions. See also Table S2 and Data S2.

ribosome-binding site (Figure 5D). To corroborate the *petF* mRNA as a direct IsaR1 target, we used the heterologous superfolder GFP (sGFP) reporter system established for the verification of sRNA targets in enterobacteria [26] and cyanobacteria [27]. The co-expression of IsaR1 with the *petF* 5′ UTR fused to *sgfp* in *E. coli* resulted in a significant 4.8 ± 0.8-fold repression of fluorescence (Figure 5C). Hence, the *petF* mRNA encoding Fed1 appears as a direct target of IsaR1.

The Cytochrome b_6f Complex as a Target of IsaR1

The expression of genes encoding subunits of the cytochrome b_6f complex decreased during iron starvation in WT but less so in Δ*isaR1* (Figure 5G). Out of these, *petA*, *petB*, and *petD* were identified by CopraRNA or IntaRNA as putative IsaR1 targets (Figure 3A; Data S2). IsaR1 overexpression negatively affected the *petC1A* and *petBD* transcript accumulation under non-stress conditions (Figure 5E) and led to a corresponding reduction of cytochrome f and PetC1 at the

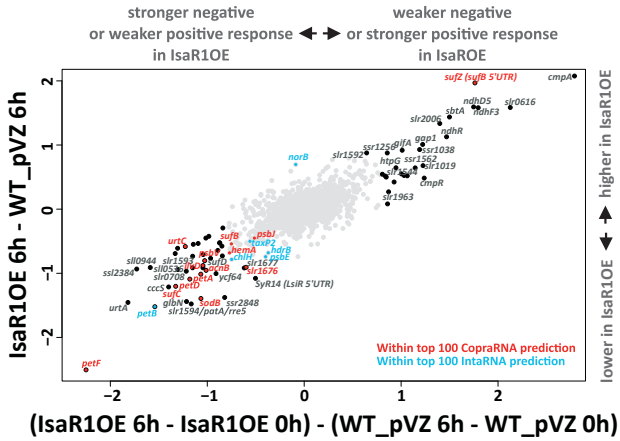

Figure 4. Transcriptome Differences in IsaR1OE and the Control after 6-Hr Pulse Expression of IsaR1, When It Was ~25-Fold Overexpressed

x axis: copper response of IsaR1OE with IsaR1 overexpression versus the copper-only response of the control. y axis: transcript levels in IsaR1OE versus that of the control strain at 6 hr after copper addition. Transcripts that showed differences before copper addition were not considered. Transcript names are shown in black for transcripts with an absolute $\log_2$-FC of $\geq$0.9 in either condition and in red or blue for CopraRNA/IntaRNA top 100 predicted targets, with an absolute FC of $\geq$0.5 in either condition. CopraRNA prediction overrules IntaRNA prediction. IsaR1 is not shown in this plot. The complete set of transcriptome differences and predicted targets is presented in Data S2, and the genome-wide expression plot for the pulsed overexpression of IsaR1 at iron-replete conditions is presented in Data S3.
See also Figure S3 and Data S2 and S3.

protein level, whereas the WT control did not show any reduction (Figures 5E and 5F). These results strongly suggest that the previously observed reduction in cytochrome b_6f complex accumulation during prolonged iron starvation (Figure 5G) [4, 5, 28] is largely mediated by IsaR1, targeting multiple different mRNAs.

Iron-Sulfur Cluster Biogenesis Is a Major Target of IsaR1

The *sufBCDS* operon encodes essential components for the biosynthesis of Fe/S clusters and appears vital for survival as the genes cannot be deleted [29]. Two transcription start sites (TSSs) were mapped for *sufB/ycf24*, 267 nt (TSS1) and 119 nt (TSS2) upstream of the start codon (Figure 6A). TSS2 was the tenth-most strongly induced TSS during iron deprivation [19], but the mRNA steady-state level was only slightly induced (Figure 6E). Moreover, our results show a repressive effect of IsaR1 on the *sufBCDS* transcript accumulation at 6 hr of ectopic overexpression of IsaR1 (Figure 6A) and the appearance of an sRNA, SufZ, that originated from TSS2 in an iron-stress-dependent manner, strictly correlating with the presence of IsaR1, as it remained undetectable in Δ*isaR1* at all times and appeared earlier in IsaR1OE (Figure 6B).

Consistently, the levels of the mRNA section of the *suf* operon and the Suf proteins remained constant at iron depletion in the WT, whereas they were strongly induced in Δ*isaR1*. SufR, the transcriptional repressor of the *sufBCDS* operon, showed an inverse response in WT and Δ*isaR1* (Figure 6E). In addition, all four proteins from the *sufBCDS* operon were strongly downregulated in IsaR1OE at 96 hr compared with the control ($\log_2$ FCs: SufB, −1.34-fold and SufC, −1.15-fold; SufD, −0.79-fold and SufS, −1.07-fold; Figure 3B). Interestingly, SufR, with a $\log_2$ factor of 1.05, was the most upregulated protein in IsaR1OE after 96 hr of induction, further illustrating the complex regulation of this operon. The first gene of the *suf* operon, *sufB*, was ranked very highly in the CopraRNA prediction (Figure 3A; Data S2). When its 5′ UTR was fused to *sgfp*, the co-expression of IsaR1 in *E. coli* resulted in a 4.6 ± 1.8-fold repression of the fluorescence signal. A change of 2 nt (GU to UA) within the predicted interaction site diminished the IsaR1-mediated repression of *sgfp* fluorescence to 2.4 ± 0.8-fold, and compensatory mutations in the 5′ UTR re-established the full 6.2 ± 3.7-fold repression (Figures 6C and S4). Thus, *sufB* was unambiguously confirmed as an IsaR1 target. We conclude that IsaR1 caps *sufBCDS* expression under iron starvation and generates SufZ as a by-product.

The Expression of Genes Encoding Several Iron-Containing Proteins and Chlorophyll and Tetrapyrrole Biosynthesis Enzymes Is Affected by IsaR1

The tetrapyrrole and chlorophyll biosynthesis enzymes encoded by *hemA* (rank 9, CopraRNA), *chlN* (rank 32, CopraRNA), and *chlH* (rank 61, IntaRNA) were potential targets of IsaR1 (Figure 3A). Both *hemA* and *chlH* responded in the IsaR1OE microarrays (Figure 4). To further verify a direct repression, we conducted an sGFP assay in *E. coli* for *hemA* and *chlN* and observed more than 2-fold repression of GFP fluorescence upon IsaR1 co-expression (Figure S4).

Several additional IsaR1 targets were suggested by prediction, transcriptomics, and proteomics (summarized in Figure 7). The mRNAs for the iron-containing form of superoxide dismutase (*sodB*), aconitate hydratase (*acnB*), and dihydroxy-acid dehydratase (*ilvD*) ranked highly in the predictions (Figure 3A), and transcript levels declined with ectopic IsaR1 expression (Figure 4). Both *sodB* and *acnB* mRNAs accumulated at an elevated level in Δ*isaR1* during iron stress (Figure 2B), similar to *petF* and the *suf* operon transcripts. Moreover, all these 5′ UTRs were controlled by IsaR1 in the sGFP assay (Figure S5), and SodB and AcnB proteins were repressed by IsaR1OE in the SRM assay; SodB by 1.27-fold and AcnB by 1.19-fold ($\log_2$-FCs; Figure 3B).

DISCUSSION

Disentanglement of Iron-Starvation Regulation

Although the physiological responses of photosynthetic organisms to iron limitation have been well studied, the knowledge of the regulatory factors behind these dynamic acclimation responses has remained scarce. The transcriptional repressor FurA cannot convey iron-starvation-dependent repression, because it requires Fe^{2+} for DNA binding. We show that the sRNA IsaR1 fulfills this repressor function in iron homeostasis. It affects the expression of several genes relevant to photosynthetic electron transfer, pigment biosynthesis, and Fe/S cluster biogenesis, and likely additional iron-cofactor-containing proteins, e.g., [Fe-Ni] hydrogenase subunits, and even regulators

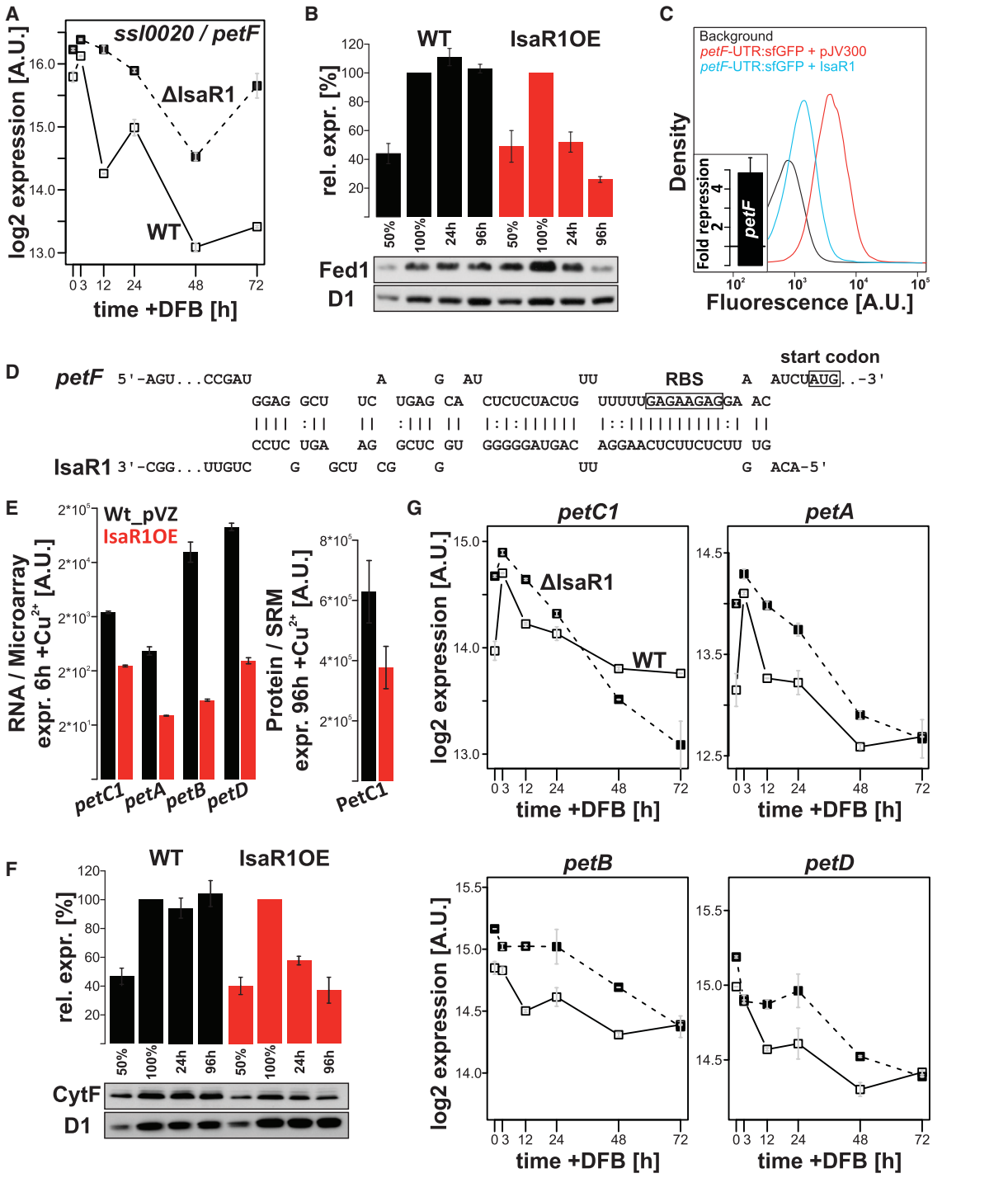

Figure 5. The Major Ferredoxin Fed1 and the Cytochrome b_6f Complex as IsaR1 Targets

(A) The *petF* gene (*ssl0020*) encodes ferredoxin I. Time course of the iron stress microarray experiment for WT and Δ*isaR1*. For each time point, the error bars were calculated from two independent microarray experiments. The transcript level began to decline 12 hr after the onset of iron stress in WT and continued to decline over 3 days. In contrast, the Δ*isaR1* mutant showed a much weaker and delayed reduction of the expression level. For additional details, see the legend for Data S1.

(B) The Fed1 protein level decreased gradually in IsaR1OE to approximately 50% after 24 hr and approximately 20% after 96 hr of Cu^{2+}-induced IsaR1 overexpression. A western blot with an antiserum against the D1 protein is shown for comparison.

(C) Verification of the IsaR1-*petF* interaction in a heterologous reporter assay. Density plot of the fluorescence of representative replicates (10,000 events each) from the flow cytometer experiment for cells carrying no GFP (background fluorescence, black) and the *petF*-UTR translationally fused to sGFP in the presence of control plasmid pJV300 (red) or in the presence of IsaR1 (blue). Inset bottom left: repression of the GFP fluorescence by IsaR1 as measured from six independent

(legend continued on next page)

involved in phototaxis. Targets that can be unambiguously assigned to IsaR1 include Fed1, cytochrome *c*6 (PetJ), the Fe/S biogenesis proteins SufBCDS, the superoxide dismutase subunit SodB, the cytochrome b_6f complex proteins PetABDC1, aconitate hydratase (AcnB), and the tetrapyrrole biosynthesis enzymes HemA and ChlN. Interestingly, *acnB* and *sodB* are also targets of RyhB in *E. coli* [30]. IsaR1 functions through a single seed region (Figure S7) that may also be used by its homologs in other cyanobacteria. An overview of the proposed IsaR1 regulon and its connections to the Fur and SufR regulons is presented in Figure 7 and Table S3.

IsaR1 and Ferredoxin

A main target of IsaR1 is Fed1, which is the major acceptor of electrons from PSI. Overexpression of IsaR1 led to decreased Fed1 amounts (Figure 5B), which can explain the observed acceptor side limitation of PSI in IsaR1OE (Figure 1E). This is highly relevant, as Fed1 is the most abundant ferredoxin, mediating several major redox processes, including the electron transfer from PSI [31] to ferredoxin NADP reductase that reduces $NADP^+$ for CO_2 fixation, nitrogen assimilation, sulfite reduction, fatty acid metabolism, and others [32]. Our results provide a mechanistic explanation for the observation that *petF* expression in cyanobacteria during iron starvation is regulated at the level of mRNA stability [33]. In addition, the SRM analysis revealed an impact of IsaR1 overexpression on other ferredoxins, Fed4 (*slr0150*, −0.79 $\log_2$-fold) and Fed5 (*slr0148*, −0.95 $\log_2$-fold). Both bind Fe/S clusters as cofactors and might be indirectly affected by the repression of their biogenesis. Notably, two more Fed and Fed-like genes (*ssr3184/fed8* and *slr1205*) appeared in the CopraRNA prediction.

Regulation of the Suf Operon

The SUF complex is the essential Fe/S cluster assembly system in *Synechocystis* 6803 [29]. Our data consistently showed *sufB* and the *suf* operon as direct targets of IsaR1. This regulation is physiologically relevant, because *suf* mRNA and protein levels were strongly correlated in all strains and conditions investigated (Figure 6C). The regulation of the capacity to produce Fe/S clusters under iron stress appears to take place mainly via the *suf* operon, because other genes involved in Fe/S biogenesis such as *sufA*, *iscA*, *nfuA*, *iscS1*, *iscS2*, *iscR*, and *rubA* [29] show only minor changes in response to iron depletion [20]. A regulator of the *suf* operon is the transcriptional repressor SufR, which is also an auto-repressor [25, 34, 35].

DNA binding by SufR depends on the presence and redox state of complexed Fe/S clusters (holo-SufR). When the capacity to provide Fe/S clusters is low, SufR appears more in the apo-form. While holo-SufR binds strongly to the *suf* promoter and represses the *suf*-operon under iron-sufficient conditions, the apo-form has a low affinity to the *suf* promoter, and *suf* operon transcription can proceed [34]. This is efficient for regulating Fe/S cluster biogenesis in iron-sufficient conditions via a feedback loop. However, when the Fe/S biogenesis capacity is limited by iron availability, this end-product repression-type regulation would lead to a constitutive transcriptional induction of the *suf* operon, which is not physiological.

Therefore, another repressor is necessary under iron-starvation conditions to control Suf protein expression. We show that IsaR1 performs this function and, thus, resembles the role of RyhB, which, under iron deprivation, controls the expression of the Fe-S cluster assembly proteins in *E. coli*, such as *iscRSUA* operon and *erpA* [30, 36, 37]. In summary, the *suf* operon is transcriptionally de-repressed during iron starvation, but this activation is counteracted by the post-transcriptional repressor IsaR1. This is in agreement with the observed repression of Suf transcripts and proteins in the SufR inactivation strain under iron depletion [35].

IsaR1 Acts on the Photosynthetic Apparatus in Three Ways

IsaR1 directly interferes with the expression of several genes encoding proteins for the photosynthetic electron transport chain. This includes the four major cytochrome b_6f proteins and the mobile electron carrier cytochrome *c*6 that transfers electrons from cytochrome b_6f to PSI and Fed1, the major electron acceptor from PSI. There is also evidence that PSI and PSII proteins such as PsbE and PsaA/B might be directly controlled by IsaR1 (Figures S4 and S6). In addition, the effects of IsaR1 on the *suf* operon and on *hemA* affect the photosynthetic apparatus indirectly. The *suf* operon encodes an essential enzymatic system for the synthesis of Fe/S clusters in *Synechocystis* 6803, whereas *hemA* encodes glutamyl-tRNA reductase, producing the first committed intermediate of the C5 pathway. This pathway is the only means for producing tetrapyrroles, chlorophylls, heme groups, and several chromophores in this organism. Chlorophyll biosynthesis is further affected by the regulation of *chlN* and *chlH*.

The availability of chlorophyll and Fe/S clusters is crucial for the assembly and stability of PSI/PSII and cytochrome b_6f

clones. The fold repression is the ratio of the GFP fluorescence of the respective translational 5′ UTR *sgfp* fusion in the presence of the control plasmid pJV300 and a plasmid for the expression of the respective IsaR1 variant, after the subtraction of the background fluorescence (details are given in Figures S4 and S5). (D) Predicted interaction between the *petF* 5′ UTR and IsaR1 (for comparison to other interactions, see Figure S7). The putative ribosome-binding site and start codon are boxed.

(E) Left: transcript levels of *petB*, *petD*, *petA*, and *petC1* detected via microarray in the WT_pVZ and IsaR1OE strains at 6 hr after induction with Cu^{2+}. The error bars were calculated from two independent microarray experiments for each time point. Right: protein expression (expr.) of PetC1 after 96-hr Cu^{2+} induction in IsaR1OE and WT_pVZ strains based on SRM assays. The error bars were calculated from three independent SRM experiments.

(F) Protein expression of cytochrome f (CytF; *petA*) in a time course experiment in WT and IsaR1OE. One representative western blot is shown. The error bars were calculated from three independent biological replicates.

(G) Transcript levels of four mRNAs encoding the four major cytochrome b_6f proteins during an iron depletion time course in WT and Δ*isaR1*. Data were taken from the iron stress microarray experiment, and the error bars were calculated from two independent experiments for each time point.

See also Figures S4, S5, and S7 and Data S1.

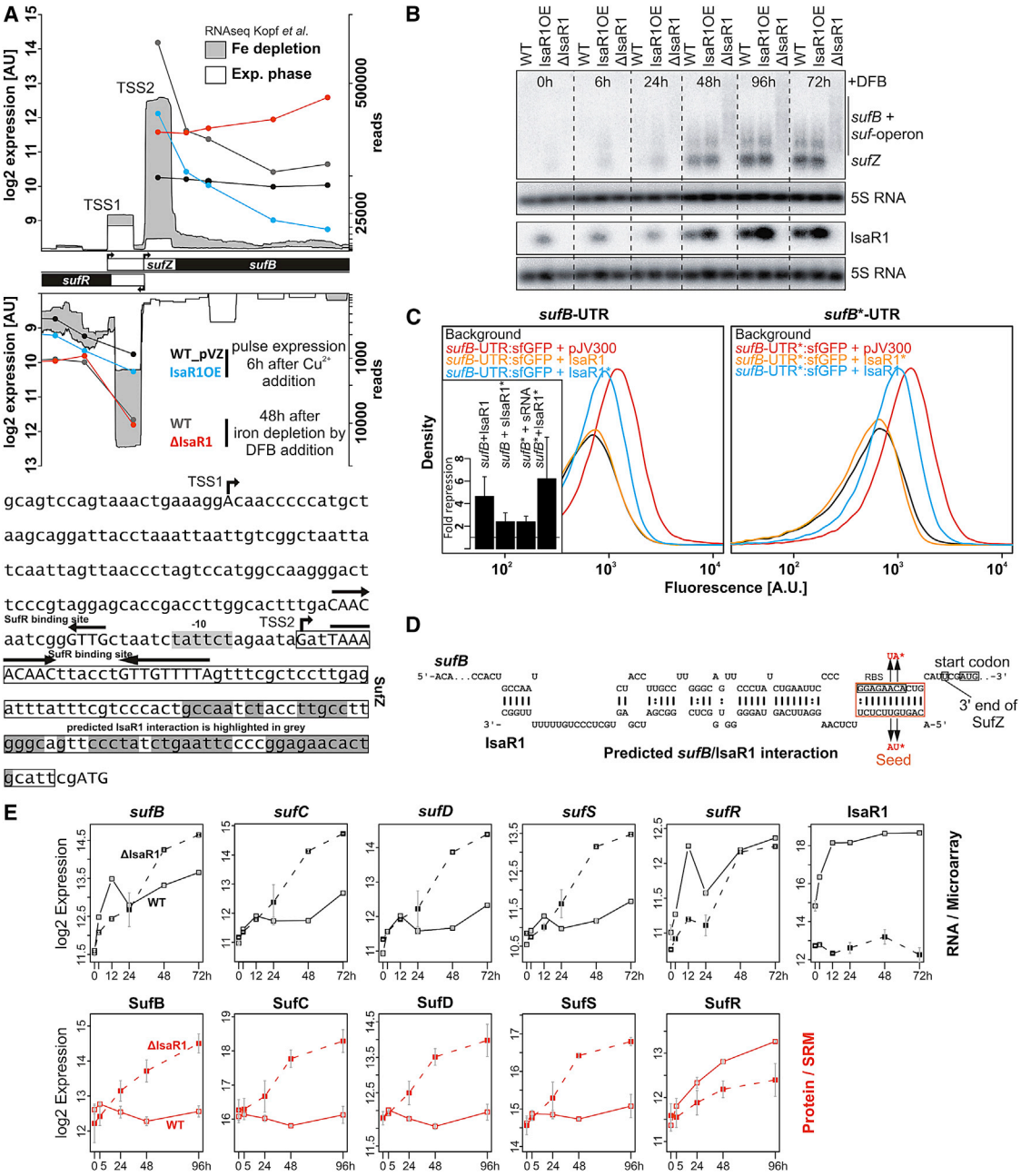

Figure 6. The *sufBCDS* Operon as a IsaR1 Target

(A) Visualization of the *sufR-sufB* intergenic and promoter region. UTRs are shown as white boxes, and genes are shown as black boxes. The read numbers for primary transcripts from an RNA-sequencing (RNA-seq) experiment after 24 hr of iron stress (gray) or exponential growth (Exp.) phase (white) were taken from reference [19] and square-root transformed (right y axis). From this mapping, TSS1 and TSS2 (bent arrows) were inferred upstream of the *sufBCDS* operon, at positions 2,871,408 and 2,871,555, respectively. The expression levels from the IsaR1 overexpression microarray experiment at 6 hr after Cu^{2+} addition (WT_pVZ: black; IsaR1OE: blue) and the iron depletion microarray experiment at 48 hr after DFB addition (WT: gray; Δ*isaR1*: red) are shown as dots (probe position) connected by lines. The numerical values for the microarray data are shown in $\log_2$ scale (left y axis). The lower portion displays the sequence of the *sufB* upstream region ending with the start codon, including both *sufB* TSSs. The proposed palindromic SufR-binding sites [34] are marked with arrows and are in uppercase. The *sufZ* sequence is boxed, and the predicted *sufB*-IsaR1 interaction is highlighted in gray.

(B) The generation of SufZ strictly depends on the presence of IsaR1. Time course of iron stress for WT, IsaR1OE, and Δ*isaR1* strains in the presence of copper ions, inducing IsaR1 expression in IsaR1OE. Upper portion: Northern hybridization with a probe to SufZ. Lower portion: hybridization with a probe to IsaR1. Note the lack of detectable SufZ accumulation in ΔIsaR1.

(C) Verification of the IsaR1-SufZ/*sufB* interaction in the sGFP reporter assay. Density plots of representative flow cytometer measurements (50,000 events each) for *E. coli* strains harboring different plasmid combinations. Left box: strain with no GFP (black); and translational fusion of WT *sufB*-UTR with sGFP in the presence of the control plasmid pJV300 (red), IsaR1 (yellow), or IsaR1 with the two point mutations shown in (D) (blue). Right box: strain with no GFP (black), translational fusion of *sufB**-UTR containing point mutations with sGFP in the presence of the control plasmid pJV300 (red), the complementary IsaR1* version

(legend continued on next page)

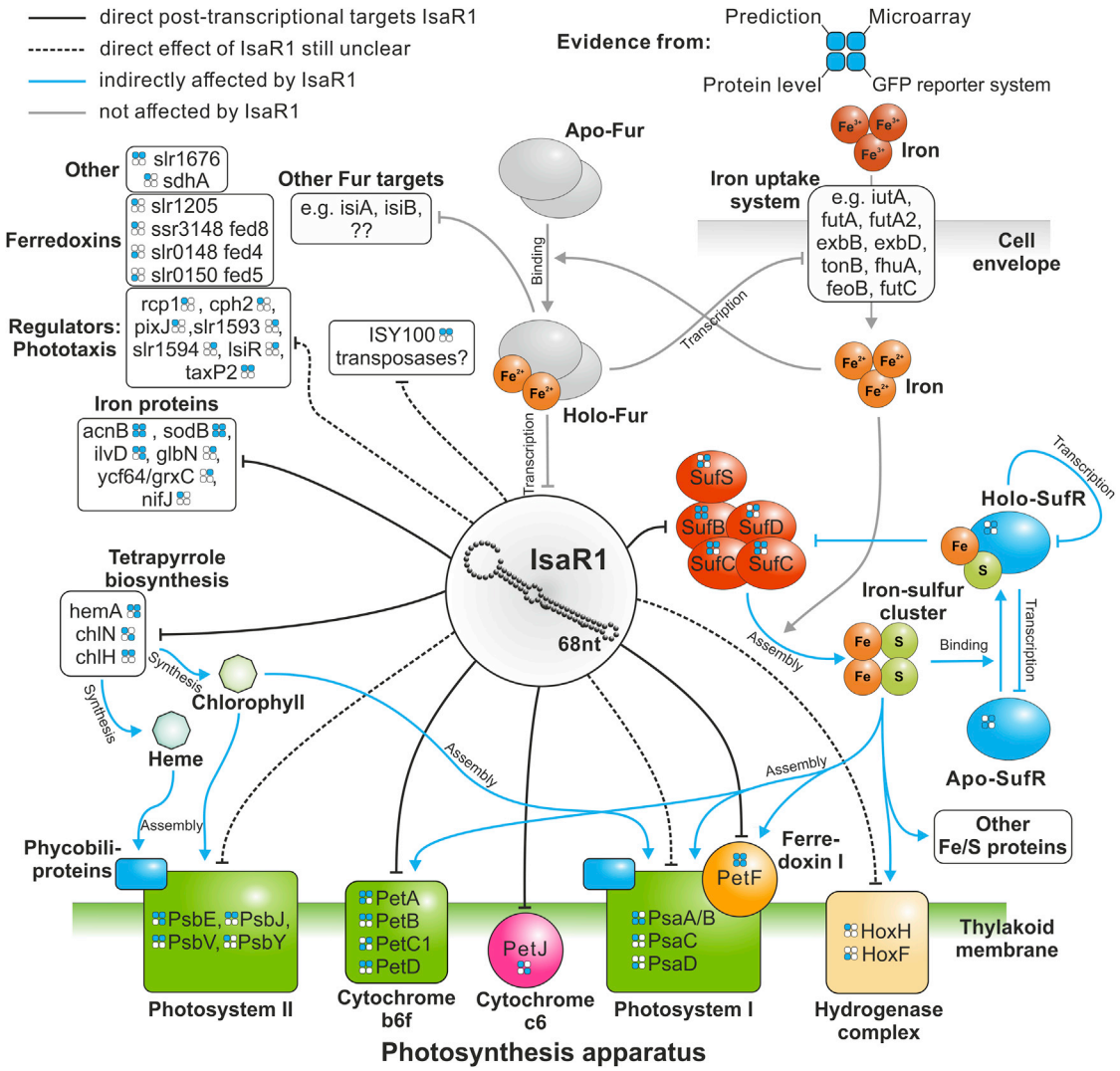

Figure 7. Model of IsaR1 Function

General overview of the IsaR1 regulon and its connections to FurA and SufR in the iron depletion stress response. The expression of IsaR1 is controlled by FurA (Figure S2). Black lines indicate verified or proposed (broken) direct post-transcriptional regulation by IsaR1. Blue lines indicate regulatory relationships indirectly affected by IsaR1. Gray lines indicate regulatory events independent of IsaR1.The source of evidence for IsaR1 targets is indicated by the filled circles for respective genes or gene products; for the underlying details, please see Table S3. In each of these panels, top left: evidence from IntaRNA or comparative CopraRNA target prediction (Figure 3A). Top right: pulse expression microarray (Figure 4) and iron depletion microarray evidence (Figures 2 and 3B). Bottom left: western blot (PetF, PetA, and PsaB) (Figure S6) or pulse IsaR1 overexpression SRM proteomic evidence (absolute $\log_2$ FC 96 hr after induction $\geq$ 0.8). Bottom right: Evidence from the GFP-reporter assay in the *E. coli* system ($\log_2$ fold repression by IsaR1 $\geq$ 1.5). See also Figures S2 and S6 and Table S3.

complexes [38, 39]. Therefore, IsaR1 impacts the photosynthetic apparatus in three fundamentally different ways: (1) by regulating certain mRNAs directly; (2) via the Fe/S cluster biosynthetic pathway; and (3) via the tetrapyrrole biosynthesis chain. The fact that a 68-nt-long riboregulator controls a network of this complexity (Figure 7) is impressive.

(yellow), or WT IsaR1 (blue). Inset in left box: fold repressions of the GFP fluorescence from the WT *sufB*-sGFP fusion with IsaR1 (*sufB* + isaR1), with IsaR1* (*sufB* + IsaR1*), and from the *sufB**-sGFP fusion in the presence of IsaR1 (*sufB** + IsaR1) or the mutated IsaR1 version (*sufB** + IsaR1*). The fold repression and the respective error were calculated from six independent clones for each strain (details are given in Figures S4A and S5A).

(D) Predicted interaction between the SufZ/*sufB* 5′ UTR and IsaR1 (for comparison to other interaction sites, see Figure S7). The seed region of interaction is boxed in orange; the start codon and ribosome-binding site are boxed in black. Point mutations are indicated by stars and orange letters.

(E) Expression of the *sufBCDS* operon and *sufR* mRNAs and of IsaR1 during the iron depletion time course in WT and Δ*isaR1* (black, upper part). The error bars are calculated from two independent microarray experiments for each time point. In the lower portion, the respective protein expression levels from the SRM experiment are shown (red). The error bars are calculated from three independent experiments for each time point (x axis: time after DFB addition, in hours). See also Figures S4, S5, and S7.

STAR★METHODS

Detailed methods are provided in the online version of this paper and include the following:

- KEY RESOURCES TABLE
- CONTACT FOR REAGENT AND RESOURCE SHARING
- EXPERIMENTAL MODEL AND SUBJECT DETAILS
  - Culture Conditions and Mutagenesis
- METHOD DETAILS
  - Spectroscopy
  - Photosynthetic Electron Transfer
  - Plasmids and Mutagenesis
  - Reporter Gene Assays
  - Construction of *E. coli* Strains Expressing His-tagged FurA
  - Expression and purification of recombinant FurA
  - Promoter Gel Shift Experiments
  - RNA Preparation and Microarray Analysis
  - Target Verification with a Heterologous Reporter System
  - Protein Extraction and Western Blots
  - SRM Triple Quadrupole Liquid Chromatography Mass Spectrometry
- QUANTIFICATION AND STATISTICAL ANALYSIS
  - Computational Prediction of IsaR1 Targets
- DATA AND SOFTWARE AVAILABILITY

SUPPLEMENTAL INFORMATION

Supplemental Information includes seven figures, three tables, and three data files and can be found with this article online at http://dx.doi.org/10.1016/j.cub.2017.04.010.

AUTHOR CONTRIBUTIONS

W.R.H. and J.G. planned the project. G.K., V.S., T.H., and M.M. generated and characterized the mutant strains. J.G. performed the bioinformatics analyses. J.G., G.K., L.V., T.H., S.K., Y.A., M.E.F., E.-M.A., and W.R.H. analyzed data. D.B. and S.K. performed *luxAB* reporter gene assays. T.K. and Y.H. performed EMSA. J.G., G.K., and L.V. prepared the figures. All authors contributed to the manuscript.

ACKNOWLEDGMENTS

We thank Gudrun Krüger and Viktoria Reimann for support in the microarray experiments and the Biocenter Finland and the Proteomics Facility of the Turku Centre for Biotechnology for support in the SRM experiments. We thank Miguel Hernández-Prieto for suggestions about Fur boxes, Christian Weingärtner for help with mutant analysis, Andreas Richter for the first target predictions, and Heiko Lokstein and Claudia Steglich for the introduction to spectroscopic analysis. This work was supported by German Federal Ministry of Education and Research grant "e:bio RNAsys" 0316165; DFG grant HE 2544/9-1 (to W.R.H.); Academy of Finland grants 253269, 271832, and 273870 (to E.M.A.); Portuguese Fundação para a Ciência e a Tecnologia grants IF/00881/2013 and UID/Multi/04326/2013–CCMAR (to M.E.F.); and European Commission FP7 Marie Curie Initial Training Network "Photo.COMM" grant 317184 (to W.R.H., E.M.A., and G.K.).

Received: January 16, 2017
Revised: April 6, 2017
Accepted: April 10, 2017
Published: May 4, 2017

REFERENCES

1. Finney, L.A., and O'Halloran, T.V. (2003). Transition metal speciation in the cell: insights from the chemistry of metal ion receptors. Science *300*, 931–936.
2. Keren, N., Aurora, R., and Pakrasi, H.B. (2004). Critical roles of bacterioferritins in iron storage and proliferation of cyanobacteria. Plant Physiol. *135*, 1666–1673.
3. Behrenfeld, M.J., and Kolber, Z.S. (1999). Widespread iron limitation of phytoplankton in the south pacific ocean. Science *283*, 840–843.
4. Fraser, J.M., Tulk, S.E., Jeans, J.A., Campbell, D.A., Bibby, T.S., and Cockshutt, A.M. (2013). Photophysiological and photosynthetic complex changes during iron starvation in *Synechocystis* sp. PCC 6803 and *Synechococcus elongatus* PCC 7942. PLoS ONE *8*, e59861.
5. Ivanov, A.G., Park, Y.I., Miskiewicz, E., Raven, J.A., Huner, N.P., and Oquist, G. (2000). Iron stress restricts photosynthetic intersystem electron transport in *Synechococcus* sp. PCC 7942. FEBS Lett. *485*, 173–177.
6. Straus, N.A. (2004). Iron deprivation: physiology and gene regulation. In The Molecular Biology of Cyanobacteria, D.A. Bryant, ed. (Kluwer Academic Publishers), pp. 731–750.
7. Guikema, J.A., and Sherman, L.A. (1983). Organization and function of chlorophyll in membranes of cyanobacteria during iron starvation. Plant Physiol. *73*, 250–256.
8. Sandmann, G. (1985). Consequences of iron deficiency on photosynthetic and respiratory electron transport in blue-green algae. Photosynth. Res. *6*, 261–271.
9. Sandmann, G., and Malkin, R. (1983). Iron-sulfur centers and activities of the photosynthetic electron transport chain in iron-deficient cultures of the blue-green alga *aphanocapsa*. Plant Physiol. *73*, 724–728.
10. Vuorijoki, L., Isojärvi, J., Kallio, P., Kouvonen, P., Aro, E.-M., Corthals, G.L., Jones, P.R., and Muth-Pawlak, D. (2016). Development of a quantitative SRM-based proteomics method to study iron metabolism of *Synechocystis* sp. PCC 6803. J. Proteome Res. *15*, 266–279.
11. Burnap, R.L., Troyan, T., and Sherman, L.A. (1993). The highly abundant chlorophyll-protein complex of iron-deficient *Synechococcus* sp. PCC7942 (CP43′) is encoded by the isiA gene. Plant Physiol. *103*, 893–902.
12. Laudenbach, D.E., and Straus, N.A. (1988). Characterization of a cyanobacterial iron stress-induced gene similar to psbC. J. Bacteriol. *170*, 5018–5026.
13. Shcolnick, S., Summerfield, T.C., Reytman, L., Sherman, L.A., and Keren, N. (2009). The mechanism of iron homeostasis in the unicellular cyanobacterium *synechocystis* sp. PCC 6803 and its relationship to oxidative stress. Plant Physiol. *150*, 2045–2056.
14. Hutber, G.N., Hutson, K.G., and Rogers, L.J. (1977). Effect of iron deficiency on levels of two ferredoxins and flavodoxin in a cyanobacterium. FEMS Microbiol. Lett. *1*, 193–196.
15. Massé, E., and Gottesman, S. (2002). A small RNA regulates the expression of genes involved in iron metabolism in *Escherichia coli*. Proc. Natl. Acad. Sci. USA *99*, 4620–4625.
16. Pecqueur, L., D'Autréaux, B., Dupuy, J., Nicolet, Y., Jacquamet, L., Brutscher, B., Michaud-Soret, I., and Bersch, B. (2006). Structural changes of *Escherichia coli* ferric uptake regulator during metal-dependent dimerization and activation explored by NMR and X-ray crystallography. J. Biol. Chem. *281*, 21286–21295.
17. Krynická, V., Tichý, M., Krafl, J., Yu, J., Kaňa, R., Boehm, M., Nixon, P.J., and Komenda, J. (2014). Two essential FtsH proteases control the level of the Fur repressor during iron deficiency in the cyanobacterium *Synechocystis* sp. PCC 6803. Mol. Microbiol. *94*, 609–624.
18. González, A., Angarica, V.E., Sancho, J., and Fillat, M.F. (2014). The FurA regulon in *Anabaena* sp. PCC 7120: in silico prediction and experimental validation of novel target genes. Nucleic Acids Res. *42*, 4833–4846.
19. Kopf, M., Klähn, S., Scholz, I., Matthiessen, J.K.F., Hess, W.R., and Voß, B. (2014). Comparative analysis of the primary transcriptome of *Synechocystis* sp. PCC 6803. DNA Res. *21*, 527–539.

20. Hernández-Prieto, M.A., Schön, V., Georg, J., Barreira, L., Varela, J., Hess, W.R., and Futschik, M.E. (2012). Iron deprivation in *Synechocystis*: inference of pathways, non-coding RNAs, and regulatory elements from comprehensive expression profiling. G3 (Bethesda) *2*, 1475–1495.
21. Kunert, A., Vinnemeier, J., Erdmann, N., and Hagemann, M. (2003). Repression by Fur is not the main mechanism controlling the iron-inducible isiAB operon in the cyanobacterium *Synechocystis* sp. PCC 6803. FEMS Microbiol. Lett. *227*, 255–262.
22. Schrader, P.S., Milligan, A.J., and Behrenfeld, M.J. (2011). Surplus photosynthetic antennae complexes underlie diagnostics of iron limitation in a cyanobacterium. PLoS ONE *6*, e18753.
23. Nsahlai, C.J., and Silver, R.P. (2003). Purification and characterization of KpsT, the ATP-binding component of the ABC-capsule exporter of *Escherichia coli* K1. FEMS Microbiol. Lett. *224*, 113–118.
24. Wright, P.R., Georg, J., Mann, M., Sorescu, D.A., Richter, A.S., Lott, S., Kleinkauf, R., Hess, W.R., and Backofen, R. (2014). CopraRNA and IntaRNA: predicting small RNA targets, networks and interaction domains. Nucleic Acids Res. *42*, W119–W123.
25. Wang, T., Shen, G., Balasubramanian, R., McIntosh, L., Bryant, D.A., and Golbeck, J.H. (2004). The sufR gene (sll0088 in *Synechocystis* sp. strain PCC 6803) functions as a repressor of the sufBCDS operon in iron-sulfur cluster biogenesis in cyanobacteria. J. Bacteriol. *186*, 956–967.
26. Corcoran, C.P., Podkaminski, D., Papenfort, K., Urban, J.H., Hinton, J.C.D., and Vogel, J. (2012). Superfolder GFP reporters validate diverse new mRNA targets of the classic porin regulator, MicF RNA. Mol. Microbiol. *84*, 428–445.
27. Georg, J., Dienst, D., Schürgers, N., Wallner, T., Kopp, D., Stazic, D., Kuchmina, E., Klähn, S., Lokstein, H., Hess, W.R., and Wilde, A. (2014). The small regulatory RNA SyR1/PsrR1 controls photosynthetic functions in cyanobacteria. Plant Cell *26*, 3661–3679.
28. Sandström, S., Ivanov, A.G., Park, Y.-I., Oquist, G., and Gustafsson, P. (2002). Iron stress responses in the cyanobacterium *Synechococcus* sp. PCC7942. Physiol. Plant. *116*, 255–263.
29. Balasubramanian, R., Shen, G., Bryant, D.A., and Golbeck, J.H. (2006). Regulatory roles for IscA and SufA in iron homeostasis and redox stress responses in the cyanobacterium *Synechococcus* sp. strain PCC 7002. J. Bacteriol. *188*, 3182–3191.
30. Massé, E., Vanderpool, C.K., and Gottesman, S. (2005). Effect of RyhB small RNA on global iron use in *Escherichia coli*. J. Bacteriol. *187*, 6962–6971.
31. Lelong, C., Boekema, E.J., Kruip, J., Bottin, H., Rögner, M., and Sétif, P. (1996). Characterization of a redox active cross-linked complex between cyanobacterial photosystem I and soluble ferredoxin. EMBO J. *15*, 2160–2168.
32. Cassier-Chauvat, C., and Chauvat, F. (2014). Function and regulation of ferredoxins in the cyanobacterium, *Synechocystis* PCC6803: recent advances. Life (Basel) *4*, 666–680.
33. Bovy, A., de Vrieze, G., Lugones, L., van Horssen, P., van den Berg, C., Borrias, M., and Weisbeek, P. (1993). Iron-dependent stability of the ferredoxin I transcripts from the cyanobacterial strains *Synechococcus* species PCC 7942 and *Anabaena* species PCC 7937. Mol. Microbiol. *7*, 429–439.
34. Shen, G., Balasubramanian, R., Wang, T., Wu, Y., Hoffart, L.M., Krebs, C., Bryant, D.A., and Golbeck, J.H. (2007). SufR coordinates two [4Fe-4S]2+, 1+ clusters and functions as a transcriptional repressor of the sufBCDS operon and an autoregulator of sufR in cyanobacteria. J. Biol. Chem. *282*, 31909–31919.
35. Vuorijoki, L., Tiwari, A., Kallio, P., and Aro, E.-M. (2017). Inactivation of iron-sulfur cluster biogenesis regulator SufR in Synechocystis sp. PCC 6803 induces unique iron-dependent protein-level responses. Biochim. Biophys. Acta *1861* (5 Pt A), 1085–1098.
36. Desnoyers, G., Morissette, A., Prévost, K., and Massé, E. (2009). Small RNA-induced differential degradation of the polycistronic mRNA iscRSUA. EMBO J. *28*, 1551–1561.
37. Mandin, P., Chareyre, S., and Barras, F. (2016). A regulatory circuit composed of a transcription factor, IscR, and a regulatory RNA, RyhB, controls Fe-S cluster delivery. MBio *7*, e00966-16.
38. Kopečná, J., Sobotka, R., and Komenda, J. (2013). Inhibition of chlorophyll biosynthesis at the protochlorophyllide reduction step results in the parallel depletion of Photosystem I and Photosystem II in the cyanobacterium *Synechocystis* PCC 6803. Planta *237*, 497–508.
39. Touraine, B., Boutin, J.-P., Marion-Poll, A., Briat, J.-F., Peltier, G., and Lobréaux, S. (2004). Nfu2: a scaffold protein required for [4Fe-4S] and ferredoxin iron-sulphur cluster assembly in Arabidopsis chloroplasts. Plant J. *40*, 101–111.
40. Trautmann, D., Voss, B., Wilde, A., Al-Babili, S., and Hess, W.R. (2012). Microevolution in cyanobacteria: re-sequencing a motile substrain of *Synechocystis* sp. PCC 6803. DNA Res. *19*, 435–448.
41. Rippka, R., Deruelles, J., Waterbury, J.B., Herdman, M., and Stanier, R.Y. (1979). Generic assignments, strain histories and properties of pure cultures of cyanobacteria. J. Gen. Microbiol. *111*, 1–61.
42. Shcolnick, S., Shaked, Y., and Keren, N. (2007). A role for mrgA, a DPS family protein, in the internal transport of Fe in the cyanobacterium *Synechocystis* sp. PCC6803. Biochim. Biophys. Acta *1767*, 814–819.
43. Mitschke, J., Georg, J., Scholz, I., Sharma, C.M., Dienst, D., Bantscheff, J., Voss, B., Steglich, C., Wilde, A., Vogel, J., and Hess, W.R. (2011). An experimentally anchored map of transcriptional start sites in the model cyanobacterium *Synechocystis* sp. PCC6803. Proc. Natl. Acad. Sci. USA *108*, 2124–2129.
44. Klähn, S., Baumgartner, D., Pfreundt, U., Voigt, K., Schön, V., Steglich, C., and Hess, W.R. (2014). Alkane biosynthesis genes in cyanobacteria and their transcriptional organization. Front. Bioeng. Biotechnol. *2*, 24.
45. Hernández, J.A., López-Gomollón, S., Muro-Pastor, A., Valladares, A., Bes, M.T., Peleato, M.L., and Fillat, M.F. (2006). Interaction of FurA from Anabaena sp. PCC 7120 with DNA: a reducing environment and the presence of Mn(2+) are positive effectors in the binding to isiB and furA promoters. Biometals *19*, 259–268.
46. Pinto, F.L., Thapper, A., Sontheim, W., and Lindblad, P. (2009). Analysis of current and alternative phenol based RNA extraction methodologies for cyanobacteria. BMC Mol. Biol. *10*, 79.
47. Ritchie, M.E., Phipson, B., Wu, D., Hu, Y., Law, C.W., Shi, W., and Smyth, G.K. (2015). limma powers differential expression analyses for RNA-sequencing and microarray studies. Nucleic Acids Res. *43*, e47.
48. MacLean, B., Tomazela, D.M., Shulman, N., Chambers, M., Finney, G.L., Frewen, B., Kern, R., Tabb, D.L., Liebler, D.C., and MacCoss, M.J. (2010). Skyline: an open source document editor for creating and analyzing targeted proteomics experiments. Bioinformatics *26*, 966–968.
49. Choi, M., Chang, C.-Y., Clough, T., Broudy, D., Killeen, T., MacLean, B., and Vitek, O. (2014). MSstats: an R package for statistical analysis of quantitative mass spectrometry-based proteomic experiments. Bioinformatics *30*, 2524–2526.
50. Sharma, V., Eckels, J., Taylor, G.K., Shulman, N.J., Stergachis, A.B., Joyner, S.A., Yan, P., Whiteaker, J.R., Halusa, G.N., Schilling, B., et al. (2014). Panorama: a targeted proteomics knowledge base. J. Proteome Res. *13*, 4205–4210.

STAR★METHODS

KEY RESOURCES TABLE

REAGENT or RESOURCE	SOURCE	IDENTIFIER
Antibodies		
antiserum against the D1 protein (*psbA* gene)	Agrisera	Cat# AS11 1786
cytochrome F (*petA* gene)	Agrisera	Cat# AS06 119; RRID: AB_2162098
ferredoxin 1 (*petF*)	Agrisera	Cat# AS06 121; RRID: AB_1031650
photosystem I P700 chlorophyll a apoprotein A2 (*psaB*)	Agrisera	Cat# AS10 695; RRID: AB_10772904
anti-DIG serum, anti-digoxigenin-AP, Fab fragments	Roche	Cat# 11093274910; RRID: AB_514497
Bacterial and Virus Strains		
Synechocystis 6803 substrain PCC-M	Hess lab	[40]
Synechocystis 6803 IsaR1OE strain	this work	
Synechocystis 6803 Δ*isaR1* strain	this work	
E. coli Origami2 (DE3)	Novagen	Cat# 71345
E. coli TOP10F'	Thermo Fischer	Cat# C303003
E. coli TOP10F	Thermo Fischer	Cat# C404010
Chemicals, Peptides, and Recombinant Proteins		
desferrioxamine B (DFB)	Sigma-Aldrich	Cat# D9533
Critical Commercial Assays		
Prime STAR Mutagenesis Kit	Takara	Cat# R046A
DIG gel shift kit, 2nd generation	Roche	Cat# 03353591910
Deposited Data		
Microarray data	this work	GEO database: GSE87496
SRM data	this work	databases Panorama Public at: https://panoramaweb.org/labkey/IsaR1.url and PASSEL at http://www.peptideatlas.org/PASS/PASS00939
Recombinant DNA		
plasmid pILA	M. Hagemann, University of Rostock, Germany	[21]
pT7Blue T-vector	Novagen	Cat# 69820
vector pET28a	Novagen	Cat# 69864
Software and Algorithms		
CopraRNA	[24]	http://rna.informatik.uni-freiburg.de/CopraRNA/Input.jsp
IntaRNA	[24]	http://rna.informatik.uni-freiburg.de/IntaRNA/Input.jsp

CONTACT FOR REAGENT AND RESOURCE SHARING

Further information and requests for resources and reagents should be directed to and will be fulfilled by the Lead Contact, Wolfgang R. Hess (wolfgang.hess@biologie.uni-freiburg.de).

EXPERIMENTAL MODEL AND SUBJECT DETAILS

Culture Conditions and Mutagenesis

We used the *Synechocystis* 6803 substrain PCC-M [40], cultured on BG-11 medium [41] with reduced iron concentrations [42], supplemented by 0.75% (w/v) agar (Bacto agar, Difco) for plating. Liquid cultures were grown in BG-11 medium containing 10 mM TES buffer (pH 8.0) under continuous illumination with white light of 50 μmol photons m^{-2} s^{-1} at 30°C. Iron starvation was triggered by addition of the chelator DFB (Sigma-Aldrich) at a final concentration of 100 μM. The choice of DFB was motivated by its superior effectiveness compared with the alternative media exchange method and other chelating agents [13]. Samples were

taken before the induction of iron depletion, as well as at 3, 12, 24, 48, and 72h after induction of iron depletion. Media for mutant strains were supplemented with 40 μg mL^{-1} kanamycin or 2 μg mL^{-1} gentamicin separately, or in combination. Copper-free BG11 medium was used for cultivation of the inducible overexpression mutant IsaR1OE and the respective control strain. For induction of the *petE* promoter $CuSO_4$ was added to a final concentration of 2 μM. Different growth conditions are indicated in the respective figures.

The IsaR1OE strain was constructed by inserting *isaR1* between the P_{petE} promoter for controlled expression and the *oop* terminator for the termination of transcription. To obtain the Δ*isaR1* strain, a kanamycin resistance cassette was inserted using homologous recombination to disrupt the *isaR1* gene.

METHOD DETAILS

Spectroscopy

The absorption spectra of whole cells were recorded using an UV-2401 PC spectrophotometer (Shimadzu). For measurement of the 77K fluorescence emission spectra, the cyanobacterial cultures were adjusted to the same chlorophyll concentration (7.5 μg Chl a/mL). The samples with intact cells were rapidly frozen in liquid nitrogen. The spectra were measured using a USB4000-FL-450 spectrofluorometer (Ocean Optics) with 440 nm excitation (10 nm width). The spectra were normalized at 726 nm.

Photosynthetic Electron Transfer

The P700 and Chl a fluorescence measurements were recorded with a Dual-PAM-100 pulse amplitude modulated fluorometer (Walz, Germany). The effective yield of PSI, Y(I), was calculated as $Y(I) = (P'_m - P)/ P_m$, where P'_m represents the maximal change of the P700 signal under actinic light upon application of a saturating pulse (5,000 μmol photons m^{-2} s^{-1}, 300 ms), and P indicates the fully reduced form of P700. P_m is the maximal change of the P700 signal upon transformation of P700 from the fully reduced to the fully oxidized state, achieved by the application of a saturation pulse after pre-illumination with far-red light (720 nm, 75 W/m^{-2}). The acceptor side limitation Y(NA) was calculated as $Y(NA) = (P_m - P'_m) / P_m$. It indicates the fraction of P700 that cannot be oxidized by a saturating pulse because of the shortage of oxidized acceptors. The maximum quantum yield of PSII (F_v/F_m) was calculated as $(F_m-F_0)/F_m$, where F_m is the maximum fluorescence level measured in the presence of 20 μM DCMU, and F_0 is the fluorescence level after turning on the measurement light. The fluorescence was recorded from dark-adapted cells upon the application of 200 μmol photons m^{-2} s^{-1} red actinic light for 1 min.

Plasmids and Mutagenesis

The IsaR1OE strain was constructed as follows: The pJet1.2 plasmid was digested with *Pvu*II and *Swa*I restriction enzymes, and the 2,118 nt fragment was dephosphorylated and used for blunt-end ligation with the P*petE* fragment amplified from *Synechocystis* 6803 using primers pPetEfw and pPetErv (sequences see below). Plasmid pJet_PetE contained the *petE* promoter for the controlled expression of sRNAs and the *oop* terminator for the termination of transcription. The *isaR1* fragment was amplified with IsaR1_for and IsaR1_ecoRI_rev primers, and digested with EcoRI resulting in blunt ended 5′ and an EcoRI 3′ sticky end. The fragment was then ligated to the pJet_PetE plasmid and digested with *Pvu*II and EcoRI. The resulting P*petE-isaR1* construct was excised by *Hind*III/*Xho*I and inserted into plasmid pVZ322. The resulting plasmid, pVZ_pPetE_IsaR1, was transferred to WT cells by conjugation and exconjugants were selected on BG11 agar plates containing 2 μg mL^{-1} gentamicin. The same plasmid was used to create the strain IsaR1comp, by conjugation into strain Δ*isaR1*. A plasmid containing only the regulatory regions was generated to obtain isogenic control strains, WT_pVZ__pPetE and Δ*isaR1*_pVZ.

For construction of the Δ*isaR1* strain, regions up- and downstream of *isaR1* were amplified with primer combinations Syr22Kno_rechte_Fl_AgeI_fw and Syr22-Kno_rechte_Fl_rev (for the upstream homologous flank) and Syr22-Kno_linke_Fl_FseI_rev and Syr22-Kno_linke_Fl_fw (for the downstream homologous flank; see below for primer sequences). The flank upstream was ligated into vector pJET1.2, afterward the downstream flank was ligated into this newly created vector. Restriction enzymes *Fse*I and *Age*I were used to open the vector and insert the kanamycin resistance cassette. Transformants were selected on 50 μg mL^{-1} kanamycin.

Oligonucleotides used in this study:

Name	Sequence (5′- 3′)	Purpose
pPetEfw	taaAAGCTTgaagggatagcaagctaatttttatgacgg	P_{petE} fragment
pPetErv	taactcgagAATAAAAAACGCCCGGCGGCAACCGAGCGAATTCC AAGAGTATTcagCTGCCCATGGTATCACAATGTTTGACA	P_{petE} fragment
IsaR1_for	ACAGTGTTCTCTTCTCAAGGATTCAG	IsaR1 fragment
IsaR1_ecoRI_rev	taagaattcCTAATCAGTTTAAGGTTTTGCCGCC	IsaR1 fragment
Syr22Kno_rechte_Fl_AgeI_fw	ACCGGTCAGATTACTGCAAATTATTGTCAATATTG	Δ*isaR1*
Syr22-Kno_rechte_Fl_rev	CCTAAACCTTTCCGTGAATTGC	Δ*isaR1*
Syr22-Kno_linke_Fl_FseI_rev	GGCCGGCCCGTGTCCGTTGTTAACTTTTTGC	Δ*isaR1*

(*Continued on next page*)

Continued

Name	Sequence (5′- 3′)	Purpose
Syr22-Kno_linke_Fl_fw	GAGAATGTTGGCGGTCATCAC	Δ*isaR1*
sufZ_for	GATTAAAACAACTTACCTGTTGTTTTAG	Northern blot –SufZ and SufB
T7_sufZ_sufB_rv	TAATACGACTCACTATAGGGCGCACCACGTCTTCACTC	Northern blot –SufZ and SufB
Syr22-T7-fw	TAATACGACTCACTATAGGGCAAAAAGTTAACAACGGACACG	Northern blot IsaR1
Syr22-rev	AGTGTTCTCTTCTCAAGGATTCAG	Northern blot IsaR1
Syr22-KpnI-fw	ggtaccTCCCGATTTACTCCAGCAGGC	*luxAB* assay
Syr22-KpnI-rev	ggtaccCTACTGAATCCTTGAGAAGAGAAC	*luxAB* assay
isiA-fw*Age*I	accggtCATTGGATTAAAGCCATGAGTTG	*luxAB* assay
isiA-rev*Fse*I	ggccggccGAATCTTTAGCACTTACTCCCG	*luxAB* assay
Syr22_5_phos	ACAGTGTTCTCTTCTCAAGGATTCAG	pIsaR1
Syr22_3_xbaI	GTTTTTTCTAGACTAATCAGTTTAAGGTTTTGCCGCC	pIsaR1
IsaR1_GFP_m1_fw	ACAGTtaTCTCTTCTCAAGGATTCAGTAGGG	pIsaR1*
IsaR1_GFP_m1_rv	GAAGAGAtaACTGTGTGCTCAGTATCTTGTTATC	pIsaR1*
IsaR1_GFP_m2_fw	ACAGTGTaCcgTTCTCAAGGATTCAGTAG	pIsaR1**
IsaR1_GFP_m2_rv	TTGAGAAcgGtACACTGTGTGCTCAGTAT	pIsaR1**
ycf24_5_NsiI	TTAATGCATACAACCCCCATGCTAAGCAGG	pXG10_sufB
ycf24_3_NheI	TTAGCTAGCGGTGACAAAGCCATATTTGTAGGG	pXG10_sufB
ycf24_m1_fw	CCGGAGAtaACTGCATTCGATGAGTTC	pXG10_sufB*
ycf24_m1_rv	ATGCAGTtaTCTCCGGGGAATTCAGATAG	pXG10_sufB*
petJ_5_NsiI	TTAATGCATCTTCGCGTCTTGAAGACTTTATCCT	pXG10_petJ
petJ_3_NheI	TTAGCTAGCAGCTTGGTTGAATAATTTAAACATTAGTTCTC	pXG10_petJ
petF_5_NsiI	TTAATGCATAGTTAAGTTTTTTGAAGTAGCTCGATCTG	pXG10_petF
petF_3_NheI	TTAGCTAGCGATGGAACTTTCACCATCGGGG	pXG10_petF
sodB_5_NsiI	TTAATGCATATGGAATCCCCTATTGAGTAGAGAATT	pXG10_sodB
sodB_3_NheI	TTAGCTAGCCTCCAGGGTGCTTTTGGAAATG	pXG10_sodB
sodB_m2_fw	TTGAGTAcgGtATTTAAATTTAAATGGCTTACGCACT	pXG10_sodB**
sodB_m2_rv	TTTAAATaCcgTACTCAATAGGGGATTCCAT	pXG10_sodB**
ilvD_5_NsiI	TTAATGCATAAGCATAGATTCGCTACGAGACAG	pXG10_ilvD
ilvD_3_NheI	TTAGCTAGCATCGCCAAAACCAACGGCCCG	pXG10_ilvD
psaA_5_NsiI	TTAATGCATATGTTTGCTGAAAACGCCTATCTGTG	pXG10_psaA
psaA_3_NheI	TTAGCTAGCCTTGCCCCACTTCTCGAAGGAAG	pXG10_psaA
slr0665_5_NsiI	TTAATGCATATTCACCGTTGACCATGAACTAATATTG	pXG10_acnB
slr0665_3_NheI	TTAGCTAGCCAGTTCACATAGTTCAGTAGTCTGC	pXG10_acnB
chlN_5_NsiI	TTAATGCATTTACGATTTACCAACGATCAAGTTATTG	pXG30_chlN
chlN_5_NheII	TTAGCTAGCTTGATAAAGCCAAGATACGCAACTAATG	pXG30_chlN
hemA_5_NsiI	TTAATGCATATTAGAGAAACTTGTTTAACAAAAAACGTCG	pXG10_hemA
hemA_3_NheI	TTAGCTAGCCCGCAGATGGGTTAGCGCTTC	pXG10_hemA
psaC_5_NsiI	TTAATGCATAATCCTGACAATATTATTTTTTTCGACTTTACG	pXG10_psaC
psaC_3_NheI	TTAGCTAGCGGGCACCATTTCTAGAACATCGA	pXG10_psaC
petD_5_NsiI	TTAATGCATCACACCTTCGTGCTTCCCTG	pXG30_petD
petD_3_NheI	TTAGCTAGCGGGCTCACCATAATAGTTGTGAC	pXG30_petD
petA_5_NsiI	TTAATGCATAGCACCTGGACCGAAACCGA	pXG30_petA
petA_3_NheI	TTAGCTAGCGACGCTGACTGTGGCGATC	pXG30_petA
nifJ_5_NsiI	TTAATGCATAAGACCCAGAGAGAACGCCATG	pXG10_nifJ
nifJ_3_NheI	TTAGCTAGCGGGATAAATGGCAATCACTTCACTG	pXG10_nifJ
sdhA_5_NsiI	TTAATGCATAGGCAGGCCCCTAGGGATT	pXG10_sdhA
sdhA_3_NheI	TTAGCTAGCTTTGGTATCAGGGGCCAGACG	pXG10_sdhA
sll0041_pixJ_5_NsiI	GTTTTTATGCATCGTCTGATGACTACTCCCCGG	pXG30_pixJ
sll0041_pixJ_3_NheI	GTTTTTGCTAGCTACCTCACTTTTATCCTCTCCATCG	pXG30_pixJ

(*Continued on next page*)

Continued

Name	Sequence (5′- 3′)	Purpose
cph2_5_NsiI	GTTTTTATGCAT ACAATTTAGCTGAGTAAATTTTTTACATTTA CTTTATTC	pXG10_cph2
cph2_3_NheI	GTTTTTGCTAGCGAGGGTTTCCCGTAAAGTCAAAGC	pXG10_cph2
petB_5_NsiI	GTTTTTATGCATGAGTAGTTCTCATTTTTGCCAAGTTTGG	pXG10_petB
petB_3_NheI	GTTTTTGCTAGCAACGTATTTGCTGGCAATGTCATC	pXG10_petB
slr1593_5_NsiI	GTTTTTATGCATAGAAAATCTTAAGGTTTTCTCCTCCCC	pXG10_slr1593
slr1593_3_NheI	GTTTTTGCTAGCAGAACTATTGCTCTCCTCTGGG	pXG10_slr1593
psbE_5_NsiI	TTAATGCATACTTGCTTTGCATTTGTCAGTCAATG	pXG10_psbE
psbE_3_NheI	TTAGCTAGCACCAGCAATAAACAACATCGGGATG	pXG10_psbE
fumC_5_NsiI	TTAATGCATCTGCGCCATTTAGACCGGG	pXG30_fumC
fumC_3_NheI	TTAGCTAGCGGAACGTTGGGTTTGCGCTC	pXG30_fumC
slr0857_5_NsiI	GTTTTTATGCATAACTATGTTATCGAGAAAGAAACCGGG	pXG30_ISY100
slr0857_3_NheI	GTTTTTGCTAGC AGATTCATCTATGTAAACTATAGCTTGA CTAC	pXG30_ISY100
slr0473_5_NsiI	GTTTTTATGCATACCCAGAATATTTGGCCGTTATCGC	pXG10_cph1
slr0473_3_NheI	GTTTTTGCTAGCACCGTGGGGCTGAATCAGGTG	pXG10_cph1
NdeI-FurA-F	AACATATGTCCTACACCGCCGAT	FurA expression in *E. coli*
XhoI-FurA-R	AACTCGAGCTAGGCCAAGGAAATACT	FurA expression in *E. coli*
PisaR1-F	TTGCCCCACTCCATTTGG	gels shift
PisaR1-R	GCCGCCAAAAAAACAGGG	gels shift
IsaR1-sub-F	GTCTCCAACAATAccccccccAccccccGTAATCTGTATAG TGATTTCACAGTG	mutagenesis of P_{isaR1}
IsaR1-sub-R	GGGGGTATTGTTGGAGACATTCTCCG	mutagenesis of P_{isaR1}

Reporter Gene Assays

For the promoter assays the upstream sequences of *isaR1* (−131 to +29 referring to the first transcribed nucleotide +1 [43] and *isiA* (−295 to +38) were transcriptionally fused to *luxAB* genes. The reporter constructs were generated by PCR amplification using the oligonucleotides isiA-fwAgeI/isiA-rev/FseI (P*isiA*) and SyR22_KpnI_fw/rev (P*isaR1*) followed by digestion with KpnI and *Age*I/*Fse*I, respectively. The products were cloned into the reporter plasmid pILA [21], which was then used to transform a *Synechocystis* strain expressing *luxCDE* genes to provide the substrate for the luciferase reaction. Bioluminescence was measured as described [44]. As negative control a strain harboring promoterless *luxAB* genes was used.

Construction of *E. coli* Strains Expressing His-tagged FurA

The coding region of *furA* (*sll0567*) was amplified by PCR using the primers NdeI-FurA-F and XhoI-FurA-R, and cloned into pT7Blue T-vector (Novagen). The PCR fragments were *Nde*I/*Xho*I excised from pT7Blue and subcloned into the same restriction sites in vector pET28a (Novagen) to express proteins with an N-terminal 6xHis-tag. The expression construct was transformed into Origami2 (DE3) competent cells (Novagen).

Expression and purification of recombinant FurA

E. coli Origami2 (DE3) strains harboring the FurA expression construct, were precultured in 2 mL TB medium containing kanamycin at 37°C overnight. The preculture was seeded into 500 mL 2 × YT medium. FurA expression was induced in midlog cultures grown overnight at 15°C with 100 μM IPTG.

Purification of 6xHis-FurA protein was performed using an immobilized metal affinity-chromatography (IMAC) resin charged with cobalt. Washing was performed with phosphate buffer and protein was eluted with 300 mM imidazole. All steps were performed at 4°C on ice. For further processing, the protein was desalted and concentrations were determined with the Bradford assay.

Promoter Gel Shift Experiments

The *isaR1* promoter fragment (from nucleotide position 3,164,543 to 3,164,317 according to the numbering in CyanoBase) was PCR-amplified from genomic DNA using primer pairs PisaR1-F and PisaR1-R, and cloned into the pT7Blue T-vector (Novagen). Point mutations were introduced using the Prime STAR Mutagenesis Kit (Takara) using primer pairs IsaR1-sub-F and IsaR1-sub-R. P*isaR1* and P*isaR1*-sub fragments were PCR amplified from these two vectors using primer pairs PisaR1-F and PisaR1-R.

For digoxigenin (DIG) labeling, 3.85 pmol of PCR product (here approx. 1.5-2.5 μL) was filled up to 10 μL with H_2O and the following components were added: 4 μL each of 5x buffer and of $CoCl_2$, 1 μL each of DIG-ddUTP and of terminal transferase. The labeling

mixture was incubated at 37°C for 15 min, then 2 μL of the EDTA stop solution and 3 μL of H_2O were added. To avoid precipitation, DIG-labeled probe was buffer-exchanged into Tris-borate buffer using Zeba Desalt Spin Columns (Thermo Scientific). Binding reactions between FurA and the DIG-labeled probe were performed according to the protocol of Roche's "DIG gel shift kit, 2nd generation" and literature [45]. Samples were separated on native-polyacrylamide (4%) gels and blotted overnight on Hybond N+ nylon membrane (GE Healthcare). DIG-labelled fragments were detected with anti-DIG serum and CDP-Star.

RNA Preparation and Microarray Analysis

Synechocystis 6803 liquid cultures were collected by quenching on ice and immediate centrifugation at 4°C. The RNA was isolated as previously described [46] with an additional phenol/chloroform/isoamyl alcohol (25:24:1 v/v) extraction preceding the RNA precipitation. Templates for probe generation were prepared using PCR. For microarray analysis, 2 μg of DNA-free total RNA was labeled, and 1.65 μg of RNA was used for hybridization. The raw fluorescence data had the normexp background subtracted, and were quantile normalized. The subsequent statistical analysis of FCs and pre-processing was performed using limma [47]. Transcripts with an absolute $\log_2$-FC of ≥ 0.9 and an adjusted p value ≤ 0.05 between IsaR1OE and the control strain were taken as potential targets. Additionally, transcripts that showed a significantly different response to the copper addition were included (i.e., |(IsaR1OE 6h – IsaR1OE 0h) – (control 6h – control 0h)| > 0.9, adj. p value ≤ 0.05) (Figure 4). Furthermore, we excluded all differentially expressed genes from the 0 hr time point (IsaR1OE 0h – control 0h < 0.8) to single out targets that responded to IsaR1 overexpression. If transcripts were within the top-100 list predicted by CopraRNA or IntaRNA, we lowered the $\log_2$-FC threshold to 0.5. The full dataset is accessible from the GEO database, GEO: GSE87496.

Target Verification with a Heterologous Reporter System

We used the sGFP plasmid system [26] to test 22 mRNAs that were suggested as direct targets of IsaR1 by prediction and microarray. We started from single bacterial colonies and measured fluorescence directly using an Accuri C6 flow cytometer (BD Biosciences). The list of plasmids is given below. For each clone, the fluorescence of 50,000 events was collected. The events were individually gated for each well to retain the events with a fluorescence lower than or equal to the mean of all fluorescence values plus four times the standard deviation. The mean of the gated events was averaged for 6 independent biological replicates. The fold repression was calculated as the ratio of the mean sGFP fluorescence of the respective translational 5′UTR–sGFP fusion in the presence of the control plasmid pJV300 and a plasmid for the overexpression of the respective sRNA, after the subtraction of the background fluorescence. The background fluorescence was measured with the control plasmids pXG-0 (with a luciferase gene instead of GFP) and pJV300, from which a short nonsense transcript is transcribed instead of a specific sRNA. The error of the fold repression was calculated considering error propagation under the assumption that the values could be correlated. A fold repression of at least 1.5 was detected for 10 targets (*sufB, sodB clhN, petF, psbE, psaA, hemA, petJ, ilvD* and *acnB*). Two targets showed no effect in the heterologous system (*psaC* and *petD*). The remaining 10 constructs had fluorescence at background or slightly above the control plasmid background levels, which made it impossible to conclude a regulatory function of IsaR1. Five of these candidates showed clear repression but with high uncertainty (*cph1, ISY100, sdhA, petB, nifJ*). In the case of *hemA*, the background was not subtracted for calculation of the fold repression. The raw fluorescence data for all UTRs tested are shown in Figure S4.

List of plasmids used in this study:

Name	Origin, Marker	Comment	Reference
pJet_PetE	Amp^R	Plasmid for controlled expression of sRNAs directed by the *petE* promoter (P*petE*; activated by addition of Cu^{2+}) with no additional nucleotides at the 5′ end. The oop terminator ensures reliable termination of the overexpressed gene. Directed insertion of the gene of interest via restriction sites for *Pvu*II and EcoRI between promoter and terminator. The gene of interest should be blunt ended at 5′ and with an EcoRI 3′ sticky end.	This study
pVZ_pPetE_IsaR1	Gen^R	Plasmid used for conjugation in *Synechocystis* for generation of IsaR1OE mutant (WT background) and IsaR1comp mutant (Δ*isaR1* background). For inducible expression of IsaR1 under the control of PpetE.	This study
pVZ_pPetE	Gen^R	For generation of isogenic control strains WT_pVZ and Δ*isaR1*_pVZ.	This study
pIsaR1	ColE1, Amp^R	IsaR1 expression plasmid	This study
pIsaR1*	ColE1, Amp^R	Derivative of pIsaR1	This study
pIsaR1**	ColE1, Amp^R	Derivative of pIsaR1	This study
pXG10_sufB	pSC101*, Cm^R	sfGFP reporter plasmid. Carries the *SufB* 5′UTR and the first 60nt of the coding sequence	This study
pXG10_sufB*	pSC101*, Cm^R	Derivative of pXG10_sufB	This study
pXG10_petJ	pSC101*, Cm^R	sfGFP reporter plasmid. Carries the *petJ* 5′UTR and the first 24nt of the coding sequence	This study
pXG10_petF	pSC101*, Cm^R	sfGFP reporter plasmid. Carries the *petF* 5′UTR and the first 51nt of the coding sequence	This study
pXG10_sodB	pSC101*, Cm^R	sfGFP reporter plasmid. Carries the *sodB* 5′UTR and the first 75nt of the coding sequence	This study

(*Continued on next page*)

Continued

Name	Origin, Marker	Comment	Reference
pXG10_sodB**	pSC101*, Cm^R	Derivative of pXG10_sodB	This study
pXG10_ilvD	pSC101*, Cm^R	sfGFP reporter plasmid. Carries the *ilvD* 5′UTR and the first 90nt of the coding sequence	This study
pXG10_psaA	pSC101*, Cm^R	sfGFP reporter plasmid. Carries the *psaA* 5′UTR and the first 90nt of the coding sequence	This study
pXG10_acnB	pSC101*, Cm^R	sfGFP reporter plasmid. Carries the *acnB* 5′UTR and the first 99nt of the coding sequence	This study
pXG30_chlN	pSC101*, Cm^R	sfGFP reporter plasmid. Carries the last 102 nt of *ssr1251* the *ssr1251-chlN* intergenic region and the first 102 nt of the *chlN* coding sequence	[27]
pXG10_hemA	pSC101*, Cm^R	sfGFP reporter plasmid. Carries the *hemA* 5′UTR and the first 108 nt of the coding sequence	[27]
pXG10_psaC	pSC101*, Cm^R	sfGFP reporter plasmid. Carries the *psaC* 5′UTR and the first 90 nt of the coding sequence	This study
pXG30_petD	pSC101*, Cm^R	sfGFP reporter plasmid. Carries the last 90 nt of *slr0342* the *slr0342-petD* intergenic region and the first 90 nt of the *petD* coding sequence	This study
pXG30_petA	pSC101*, Cm^R	sfGFP reporter plasmid. Carries the last 54 nt of *petC1* the *petC1-petA* intergenic region and the first 90 nt of the *petA* coding sequence	This study
pXG10_nifJ	pSC101*, Cm^R	sfGFP reporter plasmid. Carries the *nifJ* 5′UTR and the first 90 nt of the coding sequence	This study
pXG10_sdhA	pSC101*, Cm^R	sfGFP reporter plasmid. Carries the *sdhA* 5′UTR and the first 90 nt of the coding sequence	This study
pXG30_pixJ	pSC101*, Cm^R	sfGFP reporter plasmid. Carries the last 36 nt of *pixI* the *pixI-pixJ* intergenic region and the first 177 nt of the *pixJ* coding sequence	This study
pXG10_cph2	pSC101*, Cm^R	sfGFP reporter plasmid. Carries the *cph2* 5′UTR and the first 84 nt of the coding sequence	This study
pXG10_petB	pSC101*, Cm^R	sfGFP reporter plasmid. Carries the *petB* 5′UTR and the first 99 nt of the coding sequence	This study
pXG10_slr1593	pSC101*, Cm^R	sfGFP reporter plasmid. Carries the *slr1593* 5′UTR and the first 99 nt of the coding sequence	This study
pXG10_psbE	pSC101*, Cm^R	sfGFP reporter plasmid. Carries the *psbE* 5′UTR and the first 102 nt of the coding sequence	This study
pXG30_fumC	pSC101*, Cm^R	sfGFP reporter plasmid. Carries the last 96 nt of *murA* the *murA-fumC* intergenic region and the first 90 nt of the *fumC* coding sequence	This study
pXG30_ISY100	pSC101*, Cm^R	sfGFP reporter plasmid. Carries the last 57 nt of *slr0856* and the first 60 nt of the *slr0857 (ISY100)* coding sequence	This study
pXG10_cph1	pSC101*, Cm^R	sfGFP reporter plasmid. Carries the *cph1* 5′UTR and the first 90 nt of the coding sequence	This study

Protein Extraction and Western Blots

The protein extraction followed the protocol described in Vuorijoki et al. [10]. Briefly, proteins were extracted as a whole cell lysate in extraction buffer containing 0.1 M ammonium bicarbonate (NH_4HCO_3), 8 M urea, 0.1% (w/v) Rapigest SF (Waters Corporation, Milford, MA) and 0.2 mM PMSF. The cells were disrupted in a bead beater (Mini-Bead-Beater-8, Unigenetics Instruments, India), and the protein concentration was determined using the Bradford assay. For western blots, protein samples were separated on a 12% SDS-PAGE gel and blotted to PVDF membranes (Immobilon-P; Millipore). Protein-specific antibodies were used for the immunodetection of proteins of interest.

SRM Triple Quadrupole Liquid Chromatography Mass Spectrometry

Protein extracts were reduced with 5 mM dithiothreitol (DTT; Sigma) and alkylated with 10 mM iodoacetamide (IAA; Sigma), followed by o/n acetone:ethanol precipitation at −20°C. The resulting protein pellets were digested o/n in 50 mM NH_4HCO_3 and 5% (v/v) acetonitrile (ACN) buffer with two additions of trypsin (Sequence grade Modified, Promega, Madison, WI, USA) at a 1:100 (w/w; trypsin:protein) ratio. The samples were desalted by solid-phase extraction using a 4 mm/1 mL extraction disk cartridge (Empore C18-SD, 3M).

The SRM assays were performed using a TSQ Vantage QQQ mass spectrometer (Thermo Scientific) equipped with a nanoelectrospray ionization source. The desalted peptides were separated using a nanoflow HPLC system (EasyNanoLC 1000; Thermo Scientific). One hundred-fifty ng of each unfractionated biological triplicate was injected, including the spiked-in iRT peptides (Biognosys). A 60 min non-linear gradient (5%–20% B in 35 min; 20%–35% B in 50 min; B = ACN:water, 98:5) was applied at a 300 nL/ min flow rate. Once the peptides were eluted and ionized, they were analyzed using the QQQ-MS, operated in SRM mode, as described [10]. To maintain high sensitivity in SRM measurement, scheduled assays with a 5 min retention time for each peptide were applied, resulting in a 2.5 s cycle and > 30 ms dwell time. The protein targets and respective SRM assay parameters were selected from a public dataset, available from Panorama Public (https://panoramaweb.org/labkey/Vuorijoki_et_al_2015.url) [10]. Forty-two proteins with 107 proteotypic peptides (PTPs) were quantified in the Δ*isaR* analysis and 41 proteins with 104 PTPs in the IsaR1OE analysis. The data were processed using Skyline [48], and MSstats (3.1.4) [49] was used for relative quantification. Two endogenous peptides (YEAQNIEELTAEK and TPLFNIK) of the drug sensory protein A (*dspA; sll0698*) were used to normalize the data with a global standard normalization method. The SRM result files are available from Panorama Public [50] in Skyline format (https://panoramaweb.org/labkey/IsaR1.url), and the raw data can be accessed in the PeptidesAtlas SRM Experiment Library (PASSEL).

QUANTIFICATION AND STATISTICAL ANALYSIS

Computational Prediction of IsaR1 Targets

IsaR1 target prediction was conducted using CopraRNA [24] on webserver version 2.0.3.2 with standard parameters. The 20 organisms used are highlighted in Figure S1A. An alignment of the respective IsaR1 sequences is shown in Figure S1B. The FASTA sequences of the IsaR1 homologs and the Refseq IDs of the 20 organisms are provided below. The downloadable results of the CopraRNA prediction (Data S2) include the individual whole-genome target predictions for all organisms. The respective IntaRNA prediction for *Synechocystis* 6803 (Data S2) was used for comparison with the microarray results.

IsaR1 homologs used for the CopraRNA target prediction:
> NC_000911
ACAGTGTTCTCTTCTCAAGGATTCAGTAGGGGGTGGCTCGGCGATCGAGTGCTCCCTGTTTTTTTGGC
> NC_011726
TTGTGTTCTCCTCTCAAGGATCGGCAGGTGGAATCGTTCAGGACAGACGGTTCCCCTCTTTTTTGT
> NC_011884
CAGTGTTCTCCTCTCTGAGGAATAGGCAGGTGGGGTCAGGAAGCGCGATGCCGATCGGCCCCCTGTTT
> NZ_CP007542
TAGTGTTCTCTTCTCAAGGATTCAGTAGGGGGTGGCTCGGCGATCGGGTGCTCCCTGTTTTTTTTGC
> NC_010628
CAGTGTTCTCCTCTCTTTTAAGGATCGGCAGACGGGATTAGCCAGCAGTAGCAGGCTCGTCCCTCTTTTT
> NC_014248
ACAGTGTTCTCCTCTCTTTAAAGGATCGGCAGACGGGATTGGCCAGCGGTAGCAGGCTTATCCCTCTTTTT
> NC_019780
CAGTGTTCTCCTCTCGTTAAGAAGCAAGAAGCAGGTGGGGTAAGTCCGACCCCATCTCTTTTTTTTTGCGC
> NC_019771
TAGTGTTCTCCTCTCTTTAAAGGATCGGCAGACGGGATAGCCAGCAGCAGCAGGTTTGTCCCTCTTTTTT
> NC_003272
CAGTGTTCTCCTCTCTTTAAGGATCGGCAGACGGGATTAGTCGGCGGTAGCAGGCTCATCCCTCTTTTT
> NC_019689
AAGTGTTCTCCTCTCAAGGATCGGCAGGTGGGACCGCTAAGTCAGTATAAGGGCGGCTCTCCTGT
> NC_014501
ACAGTGTTCTCCTCTCAAGGATCGGCAGGTGGGACCGCTTGGCAGTCAATAAATGCGGCTCCCCTGT
> NC_009925
ATGTGTTCTCCTCTCAGAGGATTCGGCAGGTGGGGCCAAGGCGTTAGCGCAGCTTGGTTCCATTTTTT
> NC_010547
AAGTGTTCTCCTCTCAAGGATGGATCGGCAGGTGGAATCGTTCAGCAACACAGAGACGGTTCCCCTATTT
> NC_019748
AGTGTTCTTCTCTCAAGGAATCGGCAGGCGGGATCGCGAGTCATTAAAAAAGCGACTCCCCTGTTTTT
> NC_019745
CAGTGTTCTCCTCTCTTTTAAAGATCGGCAGACGGGGTTGGTCAGCAGTAGCAGACTGATCCCTATTTTT
> NC_019695
AAGTGTTCTCCTCTCTTTAAGGATCGGCAGACGGGATTGGTCAGCAAGTGCGGCTAATCCCTATTTTTT
> NZ_CM001793
TAGTGTTCTCCTCTCTTTAAGGATCGGCAGACGGGATTAGCCAGCAGCAGCAGGCTTGTCCCTCTTTTT
> NC_019678
CAGTGTTCTCCTCTCTTTAAGGAACGGCAGGCGGGATTGGTCAGCAGTTGCGGACTTGTCCCTCTTTTT
> NC_019751
CAGTGTTCTCCTCTCTTTAAGGATCGGCAGACGGGATTAGCCAGCTTCAGCAGGCAGTCCCTCTTTTTT
> NC_010296
AGTGTTCTCCTCTTAAGGATCGGCAGTGGAACCGCGCGGCAGTCTCTAACAATGCGGTTCCCATTTTTTT

DATA AND SOFTWARE AVAILABILITY

Synechocystis 6803 IsaR1is located from positions 3164387 to 3164320 on the reverse complementary strand (GenBank file NC_000911.1). Microarray data have been deposited in the GEO database (GEO: GSE87496) and SRM data in Panorama Public and PASSEL at http://www.peptideatlas.org/PASS/PASS00939.